© 2020. Published by The Company of Biologists Ltd | Development (2020) 147, dev185033. doi:10.1242/dev.185033

RESEARCH ARTICLE

Cortical distribution of GABAergic interneurons is determined by migration time and brain size

Pietro Fazzari[1], Niall Mortimer[2,3,4,5], Odessa Yabut[6], Daniel Vogt[2,7] and Ramon Pla[2,8,*]

ABSTRACT

Cortical interneurons (CINs) originate in the ganglionic eminences (GEs) and migrate tangentially to the cortex guided by different attractive and repulsive cues. Once inside the cortex, the cellular and molecular mechanisms determining the migration of CINs along the rostrocaudal axis are less well understood. Here, we investigated the cortical distribution of CINs originating in the medial and caudal GEs at different time points. Using molecular and genetic labeling, we showed that, in the mouse, early- and late-born CINs (E12 versus E15) are differentially distributed along the rostrocaudal axis. Specifically, late-born CINs are preferentially enriched in cortical areas closer to their respective sites of origin in the medial or caudal GE. Surprisingly, our *in vitro* experiments failed to show a preferential migration pattern along the rostrocaudal axis for medial- or caudal-born CINs. Moreover, *in utero* transplantation experiments suggested that the rostrocaudal dispersion of CINs depends on the developmental stage of the host brain and is limited by the migration time and the increasing size of the developing brain. These data suggest that the embryonic expansion of the cortex contributes to the rostrocaudal distribution of CINs.

KEY WORDS: Cortex, GABAergic interneurons, Migration, Neuron

INTRODUCTION

Proper brain function requires a balanced neuronal assembly. In the cerebral cortex, projection neurons and GABAergic cortical interneurons (CINs) localize within precise cortical regions to form functional neuronal circuits (see review by Bartolini et al., 2013; Marín and Rubenstein, 2001; Tremblay et al., 2016). Projection neurons (PNs) are born in the pallial ventricular zone (VZ) of the embryonic cortex and migrate towards the cortical expanse via two different modes of radial migration: glial-guided and glial-independent radial migration, also known as locomotion and translocation, respectively (Franco et al., 2011; Gil-Sanz et al., 2013; Kriegstein and Noctor, 2004; Nadarajah and Parnavelas, 2002). By contrast, CINs are generated in the medial and caudal ganglionic eminences (MGE and CGE), transient structures of the ventral telencephalon (Batista-Brito et al., 2009; Hu et al., 2017; Rubin et al., 2010; Wonders and Anderson, 2006). From there, postmitotic CINs migrate tangentially into the developing cortex, guided by both repulsive and attractive molecules (Flames et al., 2004; Marín et al., 2010; Nóbrega-Pereira and Marín, 2009). In addition, several growth factors have been identified in the GEs as motogenic (Polleux et al., 2002; Pozas and Ibanez, 2005).

In the neocortex, CINs disperse throughout the cortex following stereotyped routes (Lopez-Bendito et al., 2008; Sanchez-Alcaniz et al., 2011). Eventually, they move radially and are distributed in a laminar and regional-specific manner across the cortex in order to form specific local connections with PNs and among themselves (Anderson et al., 2002; Celio, 1990; Fishell and Rudy, 2011; Lavdas et al., 1999; Marín and Rubenstein, 2001; Markram et al., 2004; Vogt et al., 2014). Short-term *in vitro* experiments have shown that CINs colonize the neocortex in a lateral to medial temporal gradient (Britto et al., 2006; Lourenço et al., 2012) following the progressive maturation of the cerebral cortex (Bayer and Altman, 1991). Although these observations hint at a possible relationship between region-specific CIN distribution and cortical histogenesis, the underlying mechanisms remain to be elucidated. In this respect, the rostrocaudal (R-C) distribution of CINs at different stages remains poorly understood.

Here, we investigated the processes controlling CIN dispersion into precise cortical regions. Our results indicate that CINs do not display a R-C directionality during intracortical migration. We suggest that the time of migration and expansion of the cortical volume are factors influencing the final R-C differential arrangement of CINs in the cerebral cortex.

RESULTS

Differential distribution of CINs across cortical areas

Multiple subtypes of CINs are present in the cerebral cortex and are distinguishable according to their morphological, molecular and electrophysiological properties (Kessaris et al., 2014; Markram et al., 2004; Miyoshi et al., 2010; Wonders and Anderson, 2006). However, whether CIN subtypes are distributed randomly or settle in precise regions along the R-C axis has not been fully explored. Thus, we first analyzed the expression pattern of subtype-specific CIN markers in the cortex of wild-type (WT) mice at different R-C levels to assess their cortical distribution (Fig. 1D). To account for developmental variabilities in expression previously reported (del Rio et al., 1994; Ouellet and de Villers-Sidani, 2014), we performed the analysis at two time points, postnatal day (P) 14 and P30. Specifically, we investigated the distribution of somatostatin- (SST^+) and parvalbumin-positive (PV^+) CINs, which originate primarily in the MGE (Bartolini et al., 2013; Gelman and Mar; , 2010; Hu et al., 2017; Miyoshi et al., 2007; Xu et al., 2008), and vasoactive intestinal peptide-positive (VIP^+) CINs, primarily derived from the CGE (Gelman et al., 2011; Hu et al., 2017; Miyoshi et al., 2010; Taniguchi

[1]Laboratory of Cortical Circuits in Health and Disease, CIPF Centro de Investigación Príncipe Felipe, 46012 Valencia, Spain. [2]Department of Psychiatry, Neuroscience Program and the Nina Ireland Laboratory of Developmental Neurobiology, University of California San Francisco, San Francisco, CA 94158, USA. [3]Division of Molecular Psychiatry, Center of Mental Health, University of Würzburg, 97070 Würzburg, Germany. [4]Psychiatric Genetics Unit, Group of Psychiatry, Mental Health and Addiction, Vall d'Hebron Research Institute (VHIR), Universitat Autònoma de Barcelona, 08035 Barcelona, Spain. [5]Department of Psychiatry, Hospital Universitari Vall d'Hebron, 08035 Barcelona, Spain. [6]Department of Neurology, University of California San Francisco, San Francisco, CA 94158, USA. [7]Department of Pediatrics and Human Development, Michigan State University, Grand Rapids, MI 49503, USA. [8]Instituto de investigación en discapacidades neurológicas (IDINE), University of Castile-la-Mancha, 02006 Albacete, Spain.

*Author for correspondence (ramon.pla@uclm.es)

P.F., 0000-0003-3457-9201; N.M., 0000-0003-4608-2585; O.Y., 0000-0001-9991-0167; D.V., 0000-0003-1876-5936; R.P., 0000-0003-4115-149X

Handling Editor: Paola Arlotta
Received 27 September 2019; Accepted 15 June 2020

Development (2020) 147, dev185033. doi:10.1242/dev.185033

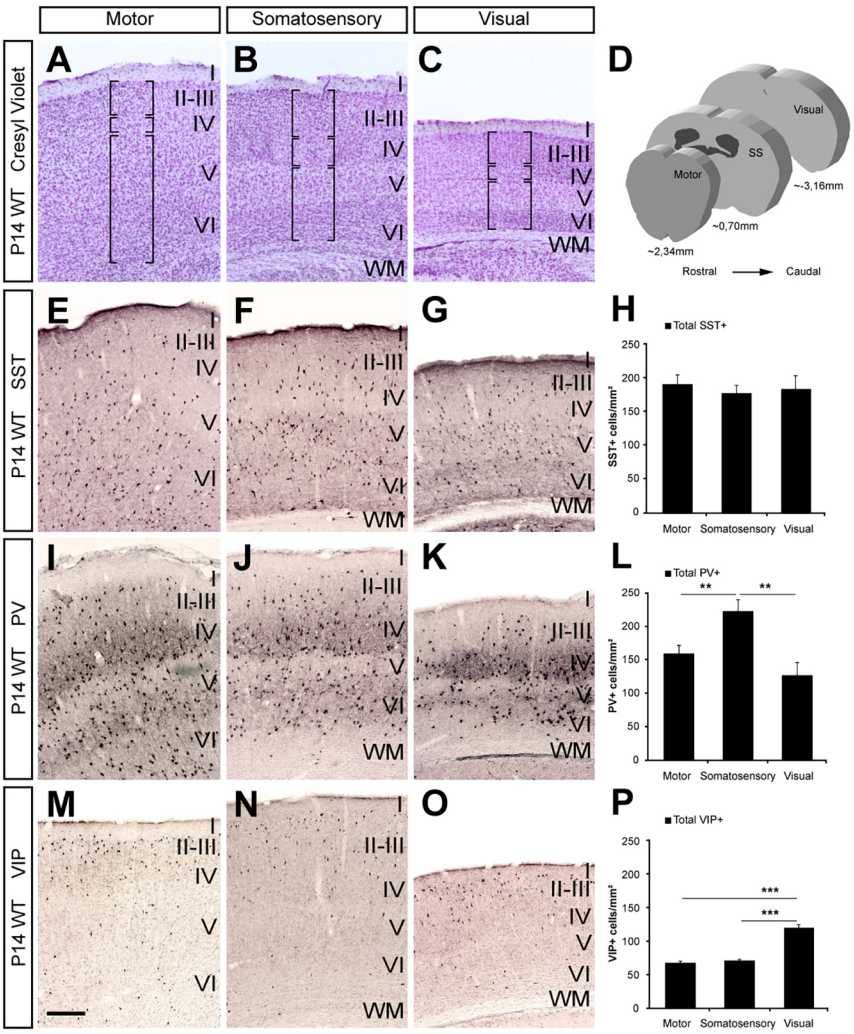

Fig. 1. Changes in CIN density along the cerebral rostrocaudal axis. Coronal sections through the motor (A,E,I,M), somatosensory (B,F,J,N) and visual (C,G,K,O) cortex of P14 wild-type mice. (A-C) Cresyl Violet-stained sections delineating specific cortical layers (in brackets) assigned in these studies. (D) The three areas studied are represented by schematic drawings of coronal sections with their corresponding level with respect to bregma. (E-G) Immunohistochemistry for SST^+ cells shows equal distribution in the three studied areas, motor (E), somatosensory (F) and visual cortex (G). (I-K) Immunohistochemistry for PV^+ cells shows preferential localization in the somatosensory cortex (J) rather than motor (I) or visual (K) cortices. However, the visual cortex (O) has a high density of VIP^+ cells compared with the motor (M) and somatosensory cortices (N). (H,L,P) Quantification of the density of SST^+ (H) (motor, 192.15±12.93 cells/mm^2; somatosensory, 178.45±13.1 cells/mm^2; visual, 183.59±21.95 cells/mm^2, P=0.59, n=7), PV^+ (L) (motor, 155.84±13.06 cells/mm^2; somatosensory, 223.04±17.21 cells/mm^2; visual, 125.42±19.57 cells/mm^2, P=0.001, n=4) and VIP^+ (P) (motor, 66.1±4.16 cells/mm^2; somatosensory, 68.98±3.24 cells/mm^2; visual, 119.40±5.18 cells/mm^2, $P=1.7\times10^{-6}$, n=6) cells in the P14 cortex. **P<0.01, ***P<0.001 (rANOVA test). Histograms show the mean± s.e.m. I-VI, cortical layers I-VI; PV, parvalbumin; SS, somatosensory; SST, somatostatin; VIP, vasointestinal peptide. Scale bar: 200 µm.

et al., 2011). Although SST^+ cells in the motor, somatosensory (SS) and visual cortex had comparable densities at P14 (Fig. 1E-H), we found that SST^+ cells were unevenly distributed between these areas at P30 (Fig. S1A-D). By contrast, PV^+ cell density was increased in the SS compared with motor and visual cortices of WT mice at P14 (Fig. 1I-L) and P30 (Fig. S1E-H). Consistent with previous studies (Nery et al., 2002; Xu et al., 2010), we found an increase in VIP^+ cell density in the visual cortex compared with motor and SS cortices in both P14 (Fig. 1M-P) and P30 WT mice (Fig. S1I-L). Together, these data suggest that CIN subtypes are not distributed equally across distinct cortical areas in the postnatal mouse brain.

Differential CIN distribution in upper layers at distinct cortical domains

The cerebral cortex is organized into layers (Fig. 1A-C), which MGE-lineage CINs settle within in an inside-out manner. Therefore early-born cells preferentially occupy the lower layers (5 and 6), whereas late-born cells tend to locate mainly in the upper layers (2/3) (Fairén et al., 1986; Miyoshi and Fishell, 2011; Pla et al., 2006; Valcanis and Tan, 2003). We wondered whether the differential densities in PV^+, SST^+ and VIP^+ CINs at P14 and P30 occurred across all layers or specific cortical layers within each cortical region. We found a significantly increase of PV^+ cell density in the superficial layers (2/3) of the SS cortex and a non-statistically significant tendency in the rest of the layers (Fig. 2A-J).These differences were also observed at P30 (Fig. S1N).

Similar to our findings above (Fig. 1H), SST^+ cell densities were comparable between cortical layers areas within each cortical region at P14 (Fig. 2K-T). Given that we found differences in the overall distribution of SST^+ cells at P30 (Fig. S1D) and because both SST^+ and PV^+ cells are MGE-derived CINs, we reasoned that SST^+ cells might also display a differential distribution at P30 in the same layers (2/3) across different cortical regions as PV^+ cells did. The analysis of the SST^+ cell distribution in layers 2/3 revealed an accumulation in SS compared with motor and visual cortex (Fig. S1M), like PV^+ cells (Fig. S1N).

In the case of VIP^+ CINs, we found differences of cell density in all cortical layers from visual cortex, compared with motor and SS cortex, although these were more evident in layers 2/3 for both P14 and P30 WT mice (Fig. 2U-DD; Fig. S1O).

Altogether, these results indicate that early- and late-born CINs tend to distribute differently in a laminar fashion along the R-C axis. MGE-derived PV^+ and SST^+ CINs were enriched in the upper layer of SS cortex. Conversely, CGE-derived VIP^+ cells appeared more enriched in layers 2/3 of the visual cortex.

Nkx2.1-lineage CINs are preferentially localized in somatosensory cortex

Given that interneuron marker expression changes over time (del Rio et al., 1994; Denaxa et al., 2012; Mardinly et al., 2016; Ouellet and de Villers-Sidani, 2014), also confirmed by our previous experiments on PV and SST expression (Fig. 1H,L; Fig. 2J,T; Fig. S1D,H,M-N), we

Development (2020) 147, dev185033. doi:10.1242/dev.185033

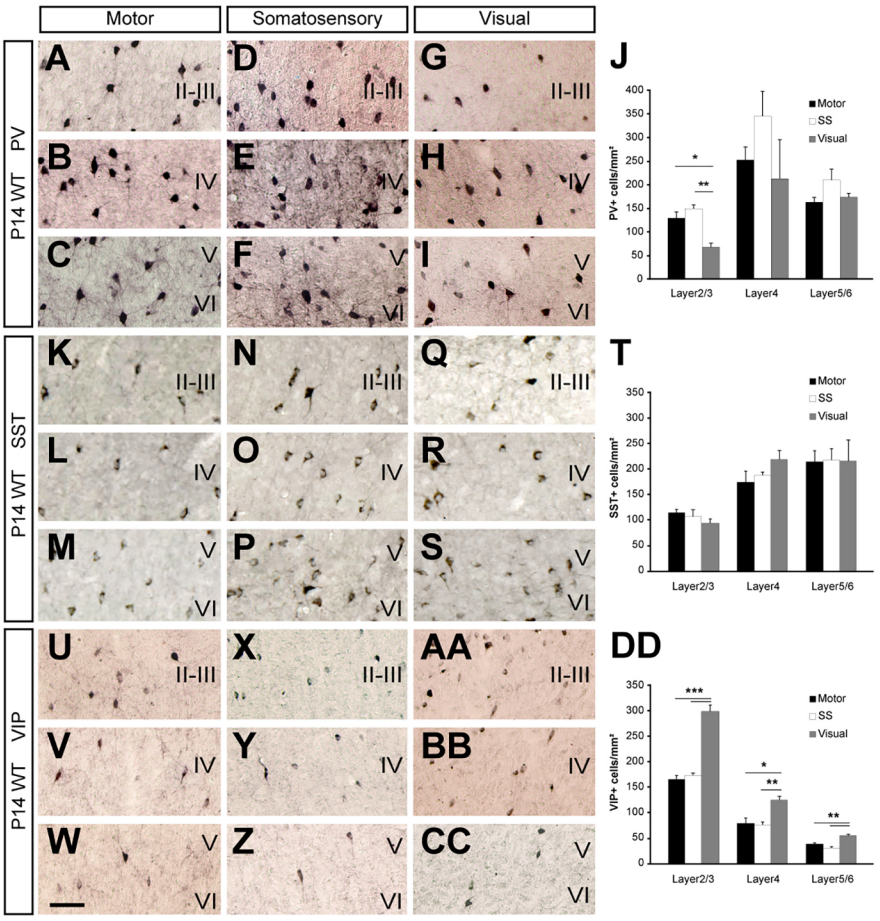

Fig. 2. Changes in CIN distribution throughout the cortex. (A-I,K-S,U-CC) Brightfield microscope images of coronal sections from cortices of P14 wild-type mice after (A-I) PV, (K-S) SST or VIP immunohistochemistry (U-CC) at motor (A-C,K-M,U-W), somatosensory (D-F, N-P,X-Z) and visual areas (G-I,Q-S,AA-CC). (J,T,DD) Cell density quantification of PV^+ (J) (layer 2/3: motor, 129.12±12.98 cells/mm^2; somatosensory, 148.87± 9.16 cells/mm^2; visual, 67.52±8.7 cells/mm^2, $P=8.9\times10^{-5}$; layer 4: motor, 252.31±27.22 cells/mm^2; somatosensory, 345.48±52.85 cells/mm^2; visual, 212.49±82.16 cells/mm^2, $P=0.15$; layer 5/6: motor, 162.97±9.43 cells/mm^2; somatosensory, 209.72± 23.28 cells/mm^2; visual, 173.55±7.95 cells/mm^2, $P=0.07$, $n=5$), SST^+ (T) (layer 2/3: motor, 114.95± 6.5 cells/mm^2; somatosensory, 107.38±13.19 cells/ mm^2; visual, 94.54±8.21 cells/mm^2, $P=0.26$; layer 4: motor, 174.59±21.85 cells/mm^2; somatosensory, 188.18±5.74 cells/mm^2; visual, 219.16±17.57 cells/ mm^2, $P=0.23$; layer 5/6: motor, 214.88±21.2 cells/ mm^2; somatosensory, 217.99±22.34 cells/mm^2; visual, 216.31±40.71 cells/mm^2, $P=0.9$, $n=5$) and VIP^+ (DD) (layer 2/3: motor, 165.17±7.5 cells/mm^2; somatosensory, 173.04±4.76 cells/mm^2; visual, 298.26±12.01 cells/mm^2, $P=5.6\times10^{-8}$; layer 4: motor, 79.03±10.66 cells/mm^2; somatosensory, 76.26± 5.81 cells/mm^2; visual, 125.09±7.18 cells/mm^2, $P=0.0006$; layer 5/6: motor, 38.82±2.93 cells/mm^2; somatosensory, 31.03±2.77 cells/mm^2; visual, 55.42± 2.31 cells/mm^2, $P=0.0001$, $n=7$). Motor (black bars), somatosensory (white bars) and visual (gray bars). *P<0.05, **P<0.01, ***P<0.001 (rANOVA test). Histograms show the mean±s.e.m. I-VI, cortical layers I-VI; PV, parvalbumin; SST, somatostatin; VIP, vasointestinal peptide. Scale bar: 50 µm.

used genetic tools to fate map the final cortical location of specific CIN subtypes carefully, based on their embryonic origin. Specifically, we crossed *Nkx2.1-Cre* (Xu et al., 2008) transgenic mice with the reporter line *Rosa 26-YFP* (Srinivas et al., 2001) to generate *Nkx2.1-Cre; Rosa 26-YFP* (*Nkx2.1-Cre; YFP*) progeny. After recombination, YFP is expressed in virtually every cell born in the MGE, including SST^+ and PV^+ CINs, except for the most dorsal MGE region corresponding to the progenitor domain of MGE 1 (Flames et al., 2007; Xu et al., 2008). Consistent with our findings on PV^+ and SST^+ cell densities, immunohistochemical analysis of the P14 *Nkx2.1-Cre; YFP* mice showed an increase in YFP^+ cell density in the upper layers of the SS versus motor cortex and a statistically significant increase compared with the upper layers of the visual cortex (Fig. 3A-D,E,G,I). The same analysis at P30 yielded similar results (Fig. 3K-N,O,Q,S). Conversely, we found no differences in YFP^+ cell densities in deeper layers at P14 or P30 (Fig. 3A-D,F,H,J,K-N,P,R,T).

CINs undergo programmed cell death between P7 and P15, leading to a 40% reduction of total CINs in the neocortex (Southwell et al., 2012). This apoptotic process might impact distinct cortical areas variably and therefore alter the R-C distribution of CINs. To test this, we analyzed the distribution of YFP^+ CINs and quantified apoptotic YFP^+ CINs at different R-C levels by co-labeling with the apoptotic marker cleaved caspase-3 at P7. Similar to our observations at P14 and P30, we observed an increase in MGE-derived YFP^+ cell density in the upper layers of the SS cortex compared with motor and visual cortices (Fig. S2A-C,D,F). Conversely, we saw an even distribution of YFP^+ cells in deep cortical layers across all cortical brain areas analyzed at P7 (Fig. S2A-C,E,G). Furthermore, the count of apoptotic YFP^+ cells co-labelled with the cleaved caspase-3 marker failed to reveal differences between the motor, SS and visual cortex at P7 (Fig. S2I-J). Our results show that the differences in CIN distribution are present in neonates and that this distribution is not caused by the programmed cell death that occurs at these ages. Incidentally, we also observed an increase in the thickness of SS and visual cortex from P7 to P30 (Fig. S2H). Altogether, our findings suggest that the differential distribution of CINs across the cortex is likely to be predicted by their embryonic origins or specific differences in migration.

Late-born MGE-derived cells are preferentially located in the somatosensory cortex

The results of the previous experiments suggest that late-born MGE-derived CINs in upper cortical layers behave in a different manner to early-born CINs. However, layer distribution does not precisely reflect the CIN birth dates, because CINs born at a specific time point can locate into different layers (Fairén et al., 1986; Hevner et al., 2004). Therefore, to determine precisely the relationship between CIN birth dates and their cortical location along the R-C axis, we performed pulse-chase experiments at E15, when most layer 2/3 CINs are born (Lopez-Bendito et al., 2008; Miyoshi et al., 2007; Pla et al., 2006; Valcanis and Tan, 2003). We injected pregnant *Nkx2.1-Cre; YFP* female mice with the thymidine analog 5-bromo-2′-deoxyuridine (BrdU) at E15 to label all cells born at this age. Immunohistochemistry for BrdU and YFP at P14 revealed that CINs born at E15 ($BrdU^+$/YFP^+) preferentially localized in the SS cortex compared with the visual and motor cortices (Fig. 4E-H). By contrast, when we carried out the same set of experiments injecting BrdU at E12 in order to mark early-born cells, we could not see any differences in the density of $BrdU^+$/YFP^+ cells between motor, SS and visual cortices (Fig. 4A-D).

Development (2020) 147, dev185033. doi:10.1242/dev.185033

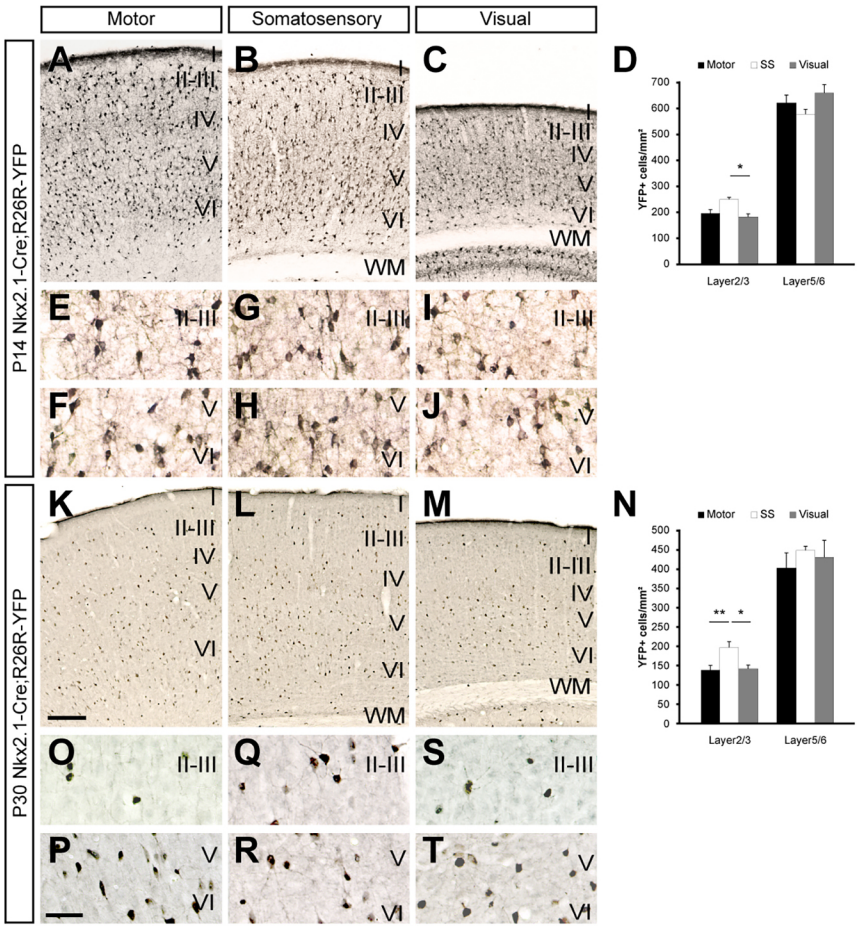

Fig. 3. MGE-derived CIN density varies along and throughout the cerebral cortex. Coronal sections through the motor (A,K), somatosensory (B,L) and visual (C,M) cortex of P14 (A-C) or P30 (K-L) *Nkx2-1-Cre; R26R-YFP* mice showing the distribution of YFP-expressing cells after YFP staining. (E-J) High-magnification images of the motor (E,F), somatosensory (G,H) and visual (I,J) P14 cortex in the supragranular (E,G,I) or infragranular (F,H,J) layers. (D) Quantification of the distribution of YFP-expressing cells in motor (black bars), somatosensory (white bars) and visual (gray bars) cortex (layer 2/3: motor, 194.62±15.01 cells/mm^2; somatosensory, 249.29±7.08 cells/mm^2; visual, 180.73±12.49 cells/mm^2, P=0.004; layer 5/6: motor, 621.06±30.29 cells/mm^2; somatosensory, 576.75±19.27 cells/mm^2; visual, 659.06±32.28 cells/mm^2, P=0.08, n=5). (O-T) High-magnification images of the motor (O,P), somatosensory (Q,R) and visual (S,T) P30 cortex in the supragranular (O,Q,S) or infragranular (P,R,T) layers. (N) Quantification of the distribution of YFP-expressing cells in motor (black bars), somatosensory (white bars) and visual (gray bars) cortex (layer 2/3: motor, 137.95±12.78 cells/mm^2; somatosensory, 196.39±15.35 cells/mm^2; visual, 141.31±9.84 cells/mm^2, P=0.0005; layer 5/6: motor, 402.33±38.32 cells/mm^2; somatosensory, 446.98±10.55 cells/mm^2; visual, 429±43.48 cells/mm^2, P=0.55, n=4). *P<0.05, **P<0.01 (rANOVA test). Histograms show the mean±sem. I-VI, cortical layers I-VI. Scale bars: (in K) 200 µm in A-C,K-M; (in P) 50 µm in E-J,O-T.

Incidentally, the total number of YFP$^+$ cells showed equal density across the three cortical areas (Fig. 4I). These findings provide evidence that the final location of MGE-derived CINs along the R-C axis is dependent on their birth date.

MGE- and CGE-derived CINs exhibit no directionality in their intracortical migration

GABAergic CINs are guided towards the cortex by several cues, including chemoattractants (Flames et al., 2004; Martini et al., 2009) or chemorrepellents (Marín, 2013; Nóbrega-Pereira et al., 2008; Zimmer et al., 2008). However, *in vitro* studies have suggested that MGE-derived CINs show no preferential dissemination in their R-C migration once inside the cortex (Lourenço et al., 2012). Therefore, to examine whether late-born CINs destined to the SS cortex migrate in a preferred direction or disperse randomly, we performed a set of cellular pathfinding assays. Specifically, we transplanted explants of MGE from embryonic day (E) 15.5 GFP-expressing embryos into E15.5 WT cortices of flat-mounted brains at different R-C locations (Fig. 5A). We found that grafted cells in the medial cortex had no spatial preference, spreading equally to the rostral and caudal sides of the transplant site (Fig. 5B,F). Moreover, we found no differences in the directionality of cell migration between the rostral and caudal side of the transplant, regardless of whether it was performed in the medial (Fig. 5B,F) or in the caudal cortex (Fig. 5D,G). We next examined whether MGE-derived CINs exclusively possessed this property or if CGE-derived CINs behaved in a similar manner when transplanted in comparable cortical regions (Fig. 5A). Given that our analysis of the VIP$^+$ CINs showed a greater density in all layers of the visual cortex (Figs 1 and 2), we expected a preferential migration of CGE-derived CINs towards the visual cortex. Surprisingly, similar to MGE transplants, cells migrating from CGE explants dispersed equally in all directions, regardless of the transplant site (Fig. 5C,E,H,I). Incidentally, a recent study showed that a subpopulation of CGE-derived CINs expressing the serotonergic ionotropic receptor 5HT3aR cross the MGE in their transit to reach the amygdala (Touzot et al., 2016). As an additional control, we performed immunohistochemical analysis of dissociated cells with 5HT3aR to determine the purity of our MGE and CGE explants. These experiments showed that our MGE explants were very pure (~90%) with very few 5HT3aR$^+$ cells present (9 out of 76; Fig. S3).

In conclusion, this set of experiments failed to show a preferential directionality in the migration of CINs. Alternatively, we reasoned that the enrichment of late-born MGE-derived cells in the SS cortex might also be caused by a reduction in migration speed, preventing cells from dispersing widely along the R-C axis. To test this, portions of MGE were removed from E12.5 and E15.5 GFP-expressing transgenic embryos and placed at the cortical VZ of sagittal host slices obtained from age-matched WT embryos (Fig. 5J). Analysis of the isochronic allotransplantation 24 h later revealed that unexpectedly, late-born cells moved a bit faster than early-born cells (Fig. 5K-M).

We next explored whether the differential velocities of E12.5- and E15.5-born CINs were cell autonomous or influenced by the cortical environment in which the cells were travelling. We performed *in vitro* experiments in which MGE explants from E12.5 and E15.5 embryos were placed in a methylcellulose matrix free of motogenic factors (Fig. 6A-C). In addition, we cultured MGE explants in Matrigel to test how the extracellular matrix affected the migration (Fig. 6D,E). Analysis of these culture

Development (2020) 147, dev185033. doi:10.1242/dev.185033

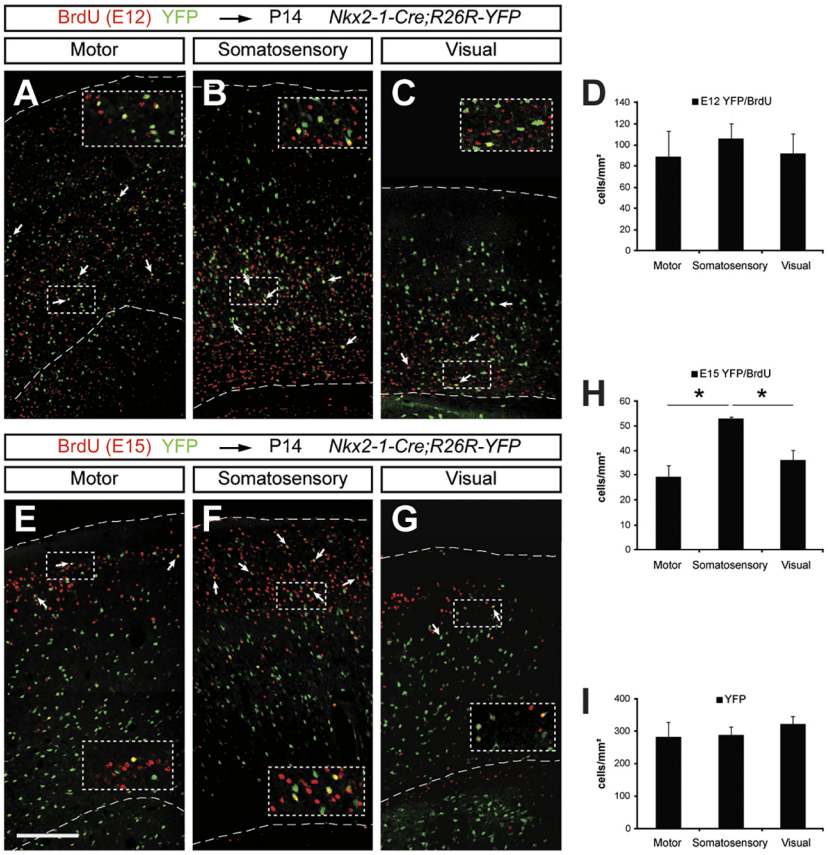

Fig. 4. Less cortical dispersion of late-born versus early-born MGE-derived CINs. (A-C,E-G) Confocal microscopy images from the cerebral cortex of P14 *Nkx2-1-Cre; R26R-YFP* mice in motor (A,E), somatosensory (B,F) and visual (C,G) areas stained for BrdU (red) and YFP (green) after BrdU injection at E12 (A-C) or E15 (E-G) (see insets). (A-C) Early-born cells ($BrdU^+/YFP^+$) are evenly dispersed in the three cortical areas (arrows), whereas late-born cells (E-G) ($BrdU^+/YFP^+$) mainly occupy somatosensory cortex, with only a few of them located in the motor and visual cortices (arrows). (D) Quantification of the distribution of E12-born cells in the motor, somatosensory and visual cortices (motor, 86.26±26.78 cells/mm^2; somatosensory, 107.99±11.56 cells/mm^2; visual, 91.82±18.37 cells/mm^2, P=0.55, n=3; 93% in layers 2/3, 5% in layer 4 and 2% in layers 2/3 across brain areas). (H) Quantification of the distribution of E15-born cells in the motor, somatosensory and visual cortices (motor, 29.34±4.36 cells/mm^2; somatosensory, 52.93±0.78 cells/mm^2; visual, 35.25± 3.19 cells/mm^2, P=0.021, n=3; 70% in layers 2/3, 20% in layer 4 and 10% in layers 2/3 across brain areas). (I) Quantification of the total YFP^+ cells in the motor, somatosensory and visual cortices (motor, 282.82± 43.94 cells/mm^2; somatosensory, 287.96±25.09 cells/mm^2; visual, 322.56±22.65 cells/mm^2, P=0.34, n=5). *P<0.05 (rANOVA test). Histograms show the mean±s.e.m. Scale bar: 200 µm.

experiments revealed that E15.5-born CINs moved slightly further than E12.5-born cells in both methylcellulose (Fig. 6C) and Matrigel matrix (Fig. 6E). In order to gain a better comprehension of the migratory behavior of early- and late-born cells, we performed a series of time-lapse videomicroscopy experiments on explants (Movies 1 and 2). These movies revealed that E12.5 cell trajectories moving out of the explant showed more meandering trajectories and longer halts between nucleokinesis compared with E15.5-born cells (Fig. S6).

Altogether, these *in vitro* assays suggest that MGE- and CGE-derived cells do not display any preferential orientation in the cortex during their migration. Moreover, compared with early-born CINs the late-born CINs display an increase in their speed along the R-C axis of the cortex.

Embryonic cortical expansion might affect rostrocaudal distribution of CINs

During embryonic development, the cortex expands rapidly along the R-C axis. As a result, late-born CINs must migrate through a larger cortex compared with CINs born at earlier stages. We hypothesized that cortical expansion might impact the R-C spreading of CINs, despite the increase in migratory speed of late-born CINs. To test this hypothesis, we first measured cortical expansion from E12.5 and E15.5 WT sagittal brain sections, unveiling that the cortical length of the neocortex doubled (Fig. 6F,G) and providing evidence that later-born CINs must traverse a longer distance.

It is noteworthy that previous studies showed that CINs share a common temporal window of ∼4-5 days of migration to reach their final location in the cortex (Bartolini et al., 2013; Hevner et al., 2004; Lopez-Bendito et al., 2008; Pla et al., 2006). Based on this information and our measurements, we developed a mathematical model that integrated cortical expansion with dispersion of CINs along the R-C axis (Fig. 6H). In this model, we considered the apparent speed of CINs that covered the maximal distance in the previous homochronic transplantation experiments *in vitro* (Fig. 5J). This mathematical model predicted that late-born CINs (E15.5), although slightly faster than early-born cells, would spread less than E12.5-born CINs along the R-C axis. Thus, given that the E15.5 cortex is twice as long as the E12.5 cortex (and still expanding), the relative distance covered by CINs along the R-C axis would be shorter. Notably, in this model we considered the speed of the 'fastest' CINs at E12.5 and E15.5. Therefore, the relative impact of cortical expansion would be even more evident if we considered that most CINs migrated more slowly (not shown).

Co-transplants *in vivo* revealed that the R-C dispersion of CINs depends on the host brain

Our working model would predict that early- and late-born CINs would spread comparably in similar conditions, particularly if given the same time and distance. In these conditions, E15.5 cells should disperse evenly along the R-C axis when transplanted into smaller brains, such as an E12.5 brain host, whereas E12.5 CINs should be enriched in the somatosensory cortex when transplanted into a bigger brain, such as an E15.5 host. To test this hypothesis, we performed *in vivo* ultrasound-guided cell transplant experiments (Pla et al., 2006). Donor pregnant females were injected with BrdU half a day before the transplant, restricting our analysis to CINs that divided last in the donor environment. Next, we pooled E12.5 GFP-expressing MGE-derived cells and E15.5 WT MGE-derived cells. Thereafter, this mixture of cells was transplanted homotopically *in utero* into the MGE of either E12.5 or E15.5 host mice, and CINs were analyzed for their spatial distribution along the R-C axis at P14 (Fig. 7A-D). The isochronic transplants of E12.5 cells into an E12.5 host and of E15.5 cells into an E15.5 host served as internal

Development (2020) 147, dev185033. doi:10.1242/dev.185033

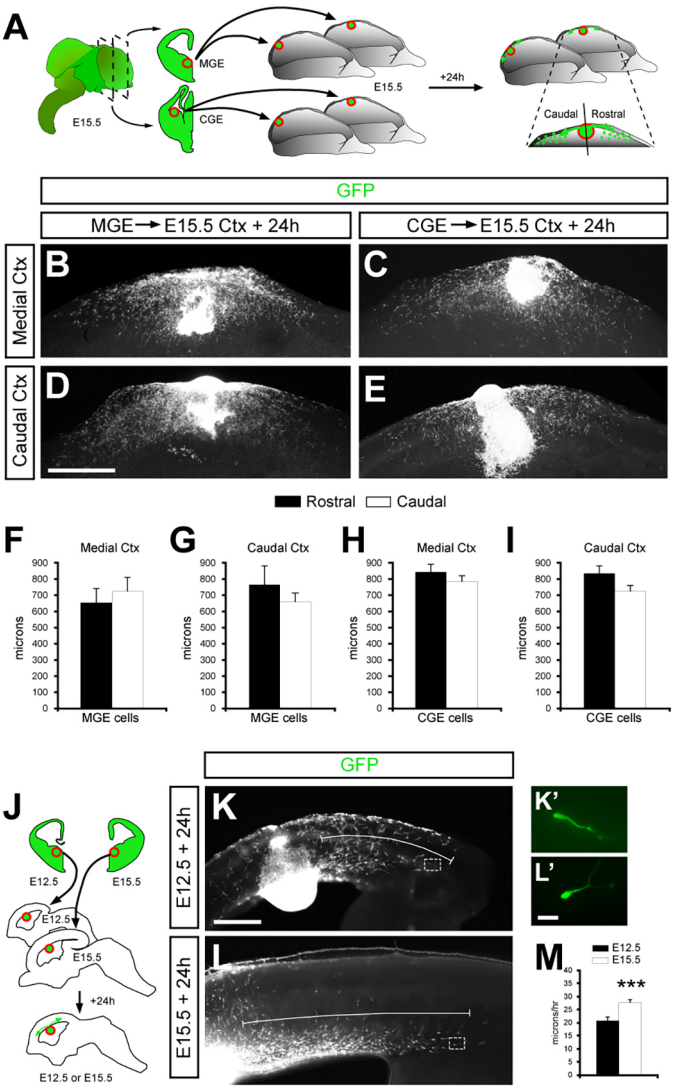

Fig. 5. CINs born at different times spread evenly in the rostrocaudal axis but exhibit different migratory speeds. (A) Schematic drawing of the experimental design followed in B-E. MGE or CGE tissue was dissected from GFP$^+$ slices of E15.5 embryos and placed in the cortex at a medial or caudal level. (B-E) Immunohistochemistry for GFP staining in E15.5 MGE (B,D) or CGE (C,E) transplanted tissue at a medial (B,C) or caudal (D,E) level in an open-book brain assay after 24 h in culture. (F-I) Quantification of the distance (in µm) traveled outside the explants in a rostral or caudal direction by MGE-derived cells [(F) rostral, 654.9±91.8 µm, n=4; caudal, 725.82±92.24 µm, n=4; P=0.6; (G) rostral, 771.48±116.29 µm, n=5; caudal, 662.74±59.32 µm, n=5; P=0.43] or CGE-derived cells [(H) rostral, 848.56±48.74 µm, n=5; caudal, 790.02±40.07 µm, n=5; P=0.38; (I) rostral, 836.21±48.9 µm, n=11; caudal, 722.57±41.57 µm, n=11; P=0.09] (unpaired Student's t-test). (J) Schema of the experimental design followed in K-M. MGE tissue (red circle) was dissected from GFP$^+$ slices of E12.5 or E15.5 embryos and placed into the ventricular zone of the cortex on slice cultures at E12.5 or E15.5, respectively. (K,L) Immunohistochemistry for GFP in E12.5 (K) or E15.5 (L) slice microtransplantation assays after 24 h in culture. White bar indicates the farthest distance traveled by the cells from the transplant. (K′,L′) High-magnification images of the boxed areas shown in K and L showing two cells in transit. (M) Quantification of the speed of E12.5 GFP$^+$ cells (black bar) and E15.5 GFP$^+$ cells (white bar) in microtransplantation assays (E12.5, 21.3± 0.21 µm/h, n=897; E15.5, 27.5±0.24 µm/h, n=797; P=9.6×10^{-77}) (Mann–Whitney U-test), n, number of cells. ***P<0.001. Histograms show the mean± s.e.m. Scale bars: (in D) 500 µm in B-E; (in K) 200 µm in K,L; (in L′) 20 µm in K′,L′.

controls. As expected, E12.5-born CINs isochronically transplanted showed a relatively even distribution across the R-C axis, whereas isochronic transplants of E15.5-born cells revealed a peak of distribution around the SS area (Fig. 7E). These experiments validated our experimental model and provided a useful reference when analyzing heterochronic transplants. Interestingly, E12.5 CINs heterochronically grafted into the E15.5 host brain showed an R-C distribution that was similar to E15.5 cells and were enriched in the medial part of the cortex (Fig. 7E,F). Conversely, E15.5 CINs transplanted into the smaller E12.5 brain spread evenly along the R-C axis, in a similar manner to the homochronic transplants of E12.5 into E12.5 (Fig. 7E,F). Collectively, these experiments showed that the age of the host brain has an important impact on the migration patterns of MGE-derived cells. Although these observations do not exclude the possibility that different CIN subtypes might also display preferential migration pathways, our findings strongly suggest that the age of the host brain, and probably its size, significantly influence the spreading of the CINs over the R-C axis.

To quantify the spreading of early- and late-born MGE CINs, we performed an extended stereological analysis of these iso- and heterochronic transplantation experiments (Fig. S4). In particular, we focused on the area of the 80th percentile, which contains 80% of the cells. The wider the spreading of the cells, the bigger the area. The area of the 80th percentile for E12.5 CIN was similar to the area of E15.5 CIN when CINs were co-transplanted simultaneously into the same host brain at both ages (Fig. 7F). Interestingly, for both E12.5- and E15.5-born cells, areas containing the 80th percentile of cells were significantly wider when CINs were transplanted into an E12.5 host brain compared with an E15.5 host brain (Fig. 7F). Moreover, the ratio between E12.5 and E15.5 host transplants was similar for both early- and late-born MGE-derived CINs (Fig. 7G). Analogous results were obtained for other percentiles. Incidentally, E15.5 CINs showed a tendency to spread further than E12.5 CINs in some percentiles (Fig. S4). These results are consistent with our *in vitro* experiments suggesting that, in the same environmental conditions, MGE-derived CINs born at E15.5 migrate faster than E12.5-born cells. These observations support the idea that the reduced spreading of late-born MGE CINs compared with early-born CINs along the R-C axis (Fig. 4) is more likely to be attributable to cortical expansion than to CIN migration speed.

To ensure that the postnatal cortical development did not alter the migration of heterochronic transplants, we also performed the analysis at P0 using E12.5 and E15.5 MGE-derived cells co-transplanted in an E15.5 host brain. As in our previous transplant experiments, we observed at P0 that both early- and late-born MGE cells were enriched at medial cortical levels, and late-born CINs spread further than E12.5 CINs in equal conditions (Fig. S5).

In conclusion, this complex set of iso- and heterochronic transplants indicated that the differential R-C distribution of early- and late-born MGE cells is not determined in a cell autonomous manner but is dependent on the characteristics of the 'host' brain at the time of migration. Altogether, these findings corroborate our mathematical model supporting the idea that cortical expansion during embryonic development contributes to the skew in the R-C distribution of CINs born at different stages.

DISCUSSION

Correct distribution of CINs in the cortex is essential for proper brain function; for instance, several neuropsychiatric disorders have been linked to deficits in CIN development (Marín, 2012). The correct balance of cortical inhibition requires not only having the right number of cells, but also that these cells integrate in the proper proportions necessary at their final destination. Several studies have focused on how CINs are generated and migrate to the cortex from

Development (2020) 147, dev185033. doi:10.1242/dev.185033

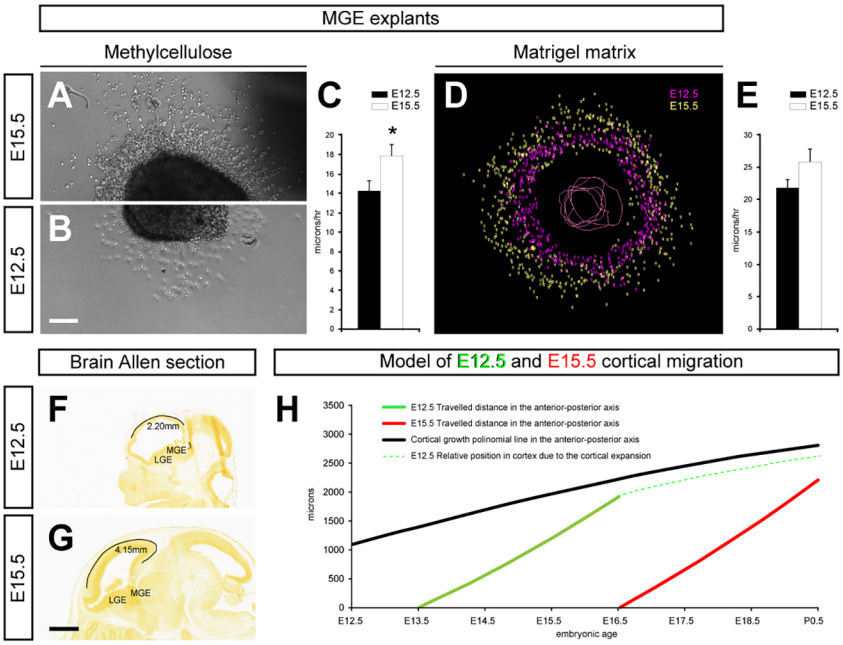

Fig. 6. CIN dispersion is influenced by velocity and cortex size. (A,B) Brightfield images of MGE explants in methylcellulose of cells born on E15.5 (A) and E12.5 (B) cultured for 24 h. (C) Quantification of the speed of E12.5-born cells (black bar) and E15.5-born cells (white bar) in methylcellulose explant assays (E12.5, 14.3±0.97 µm/h, *n*=17; E15.5, 17.8±1.17 µm/h, *n*=19; *P*=0.03). (D) Neurolucida image showing the migration of cells born on E12.5 (purple) and E15.5 (green) from explants in collagen matrix. (E) Quantification of the speed of E12.5-born cells (black bar) and E15.5-born cells (white bar) in collagen explant assays (E12.5, 21.76±1.3 µm/h, *n*=697; E15.5, 25.8±1.96 µm/h, *n*=1260; *P*=0.4). (F,G) Brain Allen microscope images from sagittal sections of E12.5 (F) and E15.5 (G) wild-type mice displaying the rostrocaudal length of the cortex (black lines) measured in millimeters (E12.5, 2.20 mm; E15.5, 4.15 mm). (H) Diagram of the mathematical model of cortical cell migration showing the migrated distance of cells born on E12.5 (green line) and E15.5 (red line) in a growing cortex (black line). **P*<0.05 (unpaired Student's *t*-test). Histograms show the mean± s.e.m. Scale bar: (in B) 80 µm in A,B; (in G) 800 µm in F,G. LGE, lateral ganglionic eminence; MGE, medial ganglionic eminence.

the GE. However, the mechanisms of intracortical migration of CINs at different developmental stages remain poorly understood (Marín, 2013). Importantly, to the best of our knowledge, intracortical migration has not yet been investigated with *in vivo* transplantation experiments as we did in the present study.

Here, we studied the processes governing intracortical migration of CIN subtypes according to their GE origins and birth date. Our results indicate that early- and late-born CINs are differentially distributed along the R-C axis of the postnatal cortex. Moreover, we found that CINs born at later stages have adapted to traversing the increasing size of the brain and that different regional cohorts of CINs, i.e. MGE or CGE derived, distribute unequally within neocortical regions closest to where they were generated.

MGE- and CGE-derived CINs distribute differently in the cortex

CINs can be classified according to their embryological origins. MGE- and CGE-derived CINs are produced in specific subpallial domains producing a broad range of molecularly distinct CIN

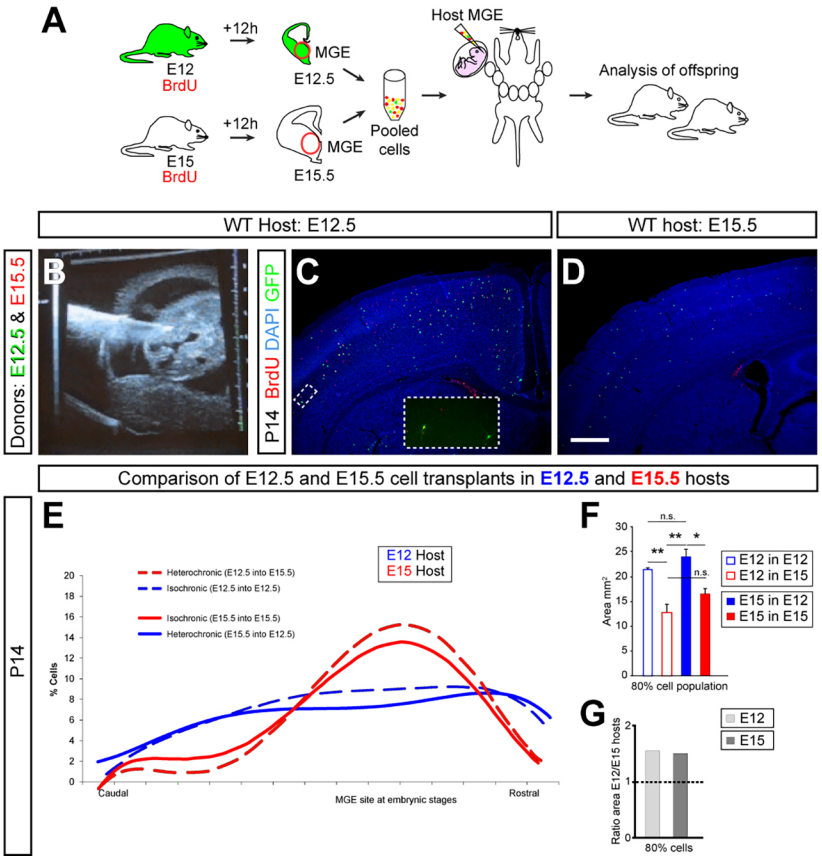

Fig. 7. Host brain characteristics modulate the intracortical migration. (A) Schematic of the experimental design. GFP$^+$ donor pregnant mice received a single injection of BrdU at E12, and wild-type donor pregnant mice received a single injection of BrdU at E15. Twelve hours after BrdU injection, the MGE was dissected from embryos and dissociated. Pooled donor MGE cells were then injected into the MGE of either E12.5 or E15.5 host embryos. Host embryos were allowed to be born and analyzed at P14. (B) Ultrasound image of a living E12.5 mouse embryo showing the moment of cell transplantation into the MGE. (C,D) Coronal sections of P14 cortices of WT mice showing the distribution of E12.5-born GFP$^+$/BrdU$^+$ and E15.5-born BrdU$^+$ cells (see insets) after transplant injections at E12.5 (C) and E15.5 (D) hosts. (E) Comparison of the rostrocaudal polynomial distribution of E12.5 interneurons transplanted into E12.5 hosts (blue dashed line), E15.5 interneurons transplanted into E15.5 hosts (red continuous line), E12.5 interneurons transplanted into E15.5 hosts (red dashed line) and E15.5 interneurons transplanted into E12.5 hosts (blue continuous line), then assessed at P14. (F) Quantification in the P14 cortex of the 80% cortical area occupied by transplanted: (1) E12.5 into E12.5 (open blue bar; 21.27± 0.4 mm^2); (2) E15.5 into E12.5 (filled blue bar; 23.87± 1.43 mm^2); (3) E12.5 into E15.5 (open red bar; 12.82± 1.6 mm^2); and (4) E15.5 into E15.5 (filled red bar; 16.56± 1.02 mm^2); *n*=3 (1 versus 2, *P*=0.003; 1 versus 3, *P*=0.45; 1 versus 4, *P*=0.078; 2 versus 3, *P*=0.001; 2 versus 4, *P*=0.22; 4 versus 3, *P*=0.012). (G) Quantification of the relative cortical area at P14 occupied by E12.5 and E15.5 interneurons transplanted into E12.5 versus E15.5 hosts. n.s. not significant, **P*<0.05, ***P*<0.01 (ANOVA test). Histograms show the mean±s.e.m. Scale bar: 400 µm.

Development (2020) 147, dev185033. doi:10.1242/dev.185033

subtypes (Flames et al., 2007; Torigoe et al., 2016; Wonders et al., 2008), each of which has a distinct way of reaching the pallium (Yozu et al., 2005). According to this, our initial analysis of subtype-specific CIN localization in the postnatal cortex identified unique distributions of each of the CIN subtypes analyzed. However despite this cellular diversity, MGE-derived CINs, both PV^+ and SST^+, reach the cortex by tangential migration using the same guiding cues and pathways (Flames et al., 2004; Nóbrega-Pereira et al., 2008). In this respect, a more detailed analysis of subtype-specific CIN localization by layers across the cortex showed distributions based only on their embryonic origins. To ensure that CIN markers were already expressed, the analyses were done at different developmental stages. In particular, MGE-derived CINs were highly enriched in the SS cortex but not in the visual and motor cortices, whereas CGE-derived CINs were enriched in the visual cortex. Consistently, we found the same results when we studied *Nkx2.1*-derived CINs, the majority of which originate from the MGE. Our observations reveal that the intracortical distribution of specific CINs along the R-C axis is correlated with their embryonic origins.

Temporal distribution of CINs across the cortex

The temporal distribution of CINs in the cortex has been studied to some extent. Previous research has focused on a single approach, such as a specific brain area, CIN subtype, cortical layers or other parameters (Celio, 1990; Hof et al., 1999; Kawaguchi and Kubota, 1997; Kubota et al., 2011; Markram et al., 2004; Miyoshi et al., 2010; Xu et al., 2010). In addition to these parameters, our data suggest that cortical size at the time when CINs are generated influences their cortical distribution and localization. BrdU pulse-chase experiments on MGE-derived cells indicate that early-born cells spread further in the cortex than late-born cells. These results also fit with our cellular density counting by layers performed on the CIN subtypes. Recent work has suggested that the subpallium contains two molecularly distinct classes of progenitor cells responsible for the generation of deep layer 5/6 CINs or superficial layer 2/3/4 CINs (Ciceri et al., 2013). According to this idea, it is plausible that behavioral differences between superficial and deep layer CINs occurred because they are derived from distinct progenitor cell subtypes (Bartolini et al., 2013; Ciceri et al., 2013). Accordingly, the results from our *in vitro* motility tests support this notion because CINs born at different time points exhibit unique migration rates even when the environment is controlled. These analyses showed that early-born CINs display more erratic trajectories and longer pauses in their movements than late-born cells. However, we cannot exclude the possibility that environmental factors, including motogenic molecules along the migration path, influence the unique migratory behavior and speed of CINs born at different stages. Future studies should focus on elucidating the underlying molecular mechanism influencing CIN subtype-specific migratory behavior.

Time and brain size control the dispersion of cortical interneurons

The idea that neuronal migration is guided by chemotaxis and predicts distinct routes of cell migration is well established. For example, CINs migrating tangentially towards the cortex are led by a combination of chemoattractive and chemorepulsive molecules (Marín et al., 2010). Moreover, different populations of CINs follow distinct migratory routes to reach the cortex and during intracortical migration (Marín, 2013; Touzot et al., 2016; Yozu et al., 2005). For instance, CGE cells reach the cortex using different pathways, or some types of SST^+ cells migrate in distinct intracortical streams, demonstrating a role in layering and perhaps in their spatial distribution (Lim et al., 2018; Pai et al., 2019; Touzot et al., 2016). By contrast, a number of *in vitro* and *in vivo* studies suggest that CGE- and MGE-derived CINs destined for distinct cortical areas, even using the same intracortical pathways, do not receive spatial information during their migration (Miyoshi and Fishell, 2011). Furthermore, there is a lack of spatial preference from isolated MGE-derived cells grafted *in vitro* in a flat-opened brain preparation (Lourenço et al., 2012). Only a few examples have been described where guidance cues play no role, one of which involves Cajal–Retzius cells. In this type of migration, also known as contact repulsion, Cajal–Retzius cells change their direction every time cell-cell contact occurs, which favors movement towards less populated areas (Villar-Cerviño et al., 2013).

Our *in vitro* experiments, in line with previous work (Lourenço et al., 2012), failed to show directional migration. It is interesting to note that in contrast to the guided migration to the cortex of MGE- and CGE-derived CINs via the medial or caudal pole of the cortex, respectively (Yozu et al., 2005), our results indicate that once the cells are in the cortex, they disperse equally along the R-C axis, independently of their birth origin. We speculate that CINs might move within the cortex driven, at least in part, by cell-cell contact repulsion. Nonetheless, it remains to be tested, and various mechanisms are likely to contribute to CIN migration. In future studies, it will be interesting to investigate these possible mechanisms and evaluate their contribution to the R-C spreading of CINs. Regardless of the migratory mechanism, our results suggest that CINs diffuse from their source, either MGE or CGE, through the cortex. These findings open interesting questions on the underlying molecular processes that control CINs in transitioning among types of migration once they cross the pallial-subpallial boundary on their way to the cortex. These may include factors such as the location where CINs enter the cortex, length of migration time, cellular speed or the size of the brain. In support of speed and brain size, we found that late-born CINs are faster than earlier born CINs. This change in the behavior of late-born CINs is likely to be an adaptation to compensate for the difficulties in reaching the furthest parts of an expanding brain.

Although CINs disperse for ∼4-5 days in the cerebral cortex, our mathematical model and the experimental results suggest that late-born CINs might not have enough time to disperse equally throughout the entire cortex. Indeed, our results show that the speed of CIN migration is not sufficient to cover the expansion of the cortex. Instead, late-born CIN subtypes from the MGE and CGE are enriched in cortical regions proximal to the subpallial domains where the CINs originated. In conclusion, we propose that cortical expansion is a crucial determinant in the distribution of distinct CIN populations across various cortical areas. These findings provide new insights into how neurodevelopmental disorders marked by abnormal brain size, such as macrocephaly and microcephaly, might contribute to observed defects in the numbers and laminar positioning of specific CIN subtypes and open interesting questions about likely synergies between cortical expansion with other mechanisms for determining the final numbers of CINs in distinct cortical regions/layers.

MATERIALS AND METHODS

Animals

All mice used in this study, including the ubiquitous green fluorescent protein (GFP)-expressing (Hadjantonakis et al., 1998), the *Nkx2.1-Cre* transgenic (Xu et al., 2008) and the Cre-dependent reporter line, *Rosa 26-YFP* (Srinivas et al., 2001), were maintained on a CD1 background. All animals were housed in a vivarium with a 12 h light, 12 h dark cycle. The day of vaginal plug was considered E0.5. All animal care and procedures were performed according to

Development (2020) 147, dev185033. doi:10.1242/dev.185033

the University of California San Francisco Laboratory Animal Research Center guidelines and the University of Castile-La Mancha guidelines under Spanish and European Union regulation.

Histology

Mice were anesthetized with an overdose of sodium pentobarbital and transcardially perfused with PBS, followed by 4% paraformaldehyde (PFA). Postnatal brains were removed, fixed for 3 h at 4°C, and cryoprotected in 30% sucrose in PBS. Frozen brains were then cut coronally on a freezing, sliding microtome at 40 µm and stored at −20°C in ethylene glycol until used. All primary and secondary antibodies were diluted in PBS containing 10% normal serum, 0.25% Triton X-100 and 2% bovine serum albumin.

The following antibodies were used: mouse anti-parvalbumin (1:3000; Swant, PV 235), rabbit anti-parvalbumin (1:5000; Swant, PV 27), goat anti-somatostatin (1:100; Santa Cruz Biotechnology, sc-7819), rabbit anti-VIP (1:300; Immunostar, 20077), chicken anti-GFP (1:2000; Aves Labs, H-1004), rabbit anti-GFP (1:2000; Invitrogen, A-11122), rat anti-bromodeoxyuridine (BrdU; 1:100; Accurate Chemical, BU1/75), goat anti-5HT3 (1:100; Abcam, ab111983) and rabbit anti-cleaved caspase-3 (1:500; Cell Signaling Technology, Asp175). The secondary antibodies for immunofluorescence were as follows: Alexa Fluor-conjugated goat anti-rabbit 488, rabbit anti-chicken 488 (both from Invitrogen), cyanine 2-conjugated donkey anti-5HT3 and cyanine 3-conjugated donkey anti-rat (both from Jackson ImmunoResearch). For indirect immunohistochemistry, sections were incubated with biotinylated secondary antibodies (Jackson ImmunoResearch), diluted 1:300, and processed by the ABC histochemical method (Vector); black reaction was obtained as described previously (Adams, 1981). For BrdU double staining, sections were first processed for GFP immunohistochemistry, fixed in 4% PFA for 50 min, then processed for BrdU staining. For immunohistochemistry of slice cultures or flat-mounted brains, tissue was fixed for 4 h in 4% PFA, washed in PBS, and incubated with primary antibodies overnight, followed by appropriate secondary antibodies. For light microscopy preparations, analyzed sections were stained with Cresyl Violet to delineate the layers of the cortex (not shown for a better visualization). Immunofluorescence specimens were counterstained with 1% 4′,6-diamidino-2-phenylindole (DAPI) to assist in the histology.

Microtransplant experiments

Donor brain slices were obtained from GFP transgenic embryos as described previously (Anderson et al., 1997). E12.5 or E15.5 MGE explants from donor slices were transplanted into the VZ of the neocortex of sagittal E12.5 or E15.5 wild-type slices, which were subsequently cultured for 24 h. Similar microtransplant experiments were performed using the MGE or CGE of E15.5 GFP-expressing embryos; in this case, donor cells were grafted into the neocortex of open-book brain preparations from E15.5 wild-type mice.

MGE explant cultures and video microscopy

MGE explants were dissected out from E12.5 and E15.5 brains and cultured on glass coverslips coated with poly-L-lysine (PLL) and laminin in Neurobasal medium containing 0.3% methylcellulose (Sigma-Aldrich). Alternatively, MGE explants were cultured in collagen matrices (BD Biosciences) as described previously (Lopez-Bendito et al., 2008). Time-lapse recordings of explants were performed using a Citation5 microscope (Biotek) in controlled temperature and CO_2 conditions. Movie frames were taken every 30 min under a ×4 phase objective. For dissociated cultures, neurons from MGE and CGE were mechanically dissociated, plated over PLL-coated coverslips and cultured in NB27 medium, as for the explants. After 24 h, cells were fixed in 4% PFA for 15 min and processed for DAPI and 5HT3aR immunohistochemistry. For quantification, several confocal images were analyzed using ImageJ software (US National Institutes of Health). Cellular trajectories from MGE explant recordings were developed using Excel software (Microsoft).

In utero transplantation

In utero ultrasound-guided transplantation of MGE-derived cells was performed as described previously (Pla et al., 2006). For each experiment, the MGEs from eight to 12 E12.5 GFP-expressing mice and E15.5 WT embryos were dissected under a stereomicroscope. Explants were washed in 0.5 ml of L-15 medium (Invitrogen) containing DNase I (100 µg/ml), and cells were mechanically dissociated by repeated pipetting. Dissociated cells were then mixed together and pelleted by centrifugation [5 min, 1000 rpm (92 ***g***)], resuspended in 6 µl of L-15 medium with DNase I, and kept on ice until injection. All donor pregnant females were given injections of BrdU 12 h before dissection. High-density cell suspensions (~25,000 cells/µl) were front-loaded into beveled glass micropipettes (~50 µm diameter) prefilled with mineral oil and mounted in a pressure microinjector (VisualSonics). Recipient pregnant females were deeply anesthetized with isoflurane, and their uterine horns were exposed and mounted under an ultrasound microscope (VisualSonics). The tip of the micropipette was inserted into the MGE under real-time ultrasound guidance, and 30–50 nl of cell suspension was injected. The position of the embryo and the path of the micropipette insertion were recorded for each embryo at the time of the injection. Embryos in which leakage to the lateral ventricle was detected were excluded from the analysis.

Image acquisition and analysis

All fluorescent and brightfield images were obtained using a DC500 camera (Leica) mounted on a DM5000B Leica fluorescence microscope or by an inverted Leica TCS SP8 confocal microscope. Brightness and contrast were adjusted using Photoshop. Cell density on DAB sections was measured with Neurolucida software (MBF Bioscience) in postnatal brains at three different R-C levels relative to bregma: ~2.3, −0.7 and −3.16 mm in motor, somatosensory and visual cortex, respectively, from both hemispheres for each replicate. For lamination counts, we used Cresyl Violet to subdivide neocortical layers.

For the quantification of $YFP^+/BrdU^+$ cells in postnatal mice, confocal tile images were manually stitched using Canvas software (Canvas GFX) were analyzed. Cells from three to five animals were counted from motor, somatosensory and visual cortex at these respective R-C levels relative to bregma: 2.3, −0.7 and −3.16 mm. Images were opened with Canvas software to delimit and measure the region of interest (ROI). All cells in the ROI were counted, then divided by the ROI area to determine cell density.

For the quantification of $GFP^+/caspase\text{-}3^+$ cells in postnatal mice, microscope images coupled using Canvas software were analyzed. Cells were counted from motor, somatosensory and visual cortex.

For the microtransplant and explant experiments, we analyzed the distance of the ~50 most dispersed cells in each slice, explant or open-book brain preparation with the Neurolucida or ImageJ software.

The analysis of the tangential dispersion of $GFP^+/BrdU^+$ and $BrdU^+$ transplanted neurons in P14 animals was carried out as described before (Lopez-Bendito et al., 2008). Briefly, all cells found in the cerebral cortex were mapped, and their mediolateral (ML) and R-C positions along the cerebral cortex were measured with respect to the midline and the rostral end of the cerebral cortex, respectively. The center-mass point for each population of cells was then calculated, defined as the intersection between a line splitting the population of cells in two halves in the R-C axis and a line splitting the population of cells in two halves in the ML axis. Then we measured the radial distance from each individual cell to the center-mass point. The entire population of transplanted cells was then ordered according to their absolute distances to the population center-mass point and divided into five groups (i.e. the 20% of cells closest to the center-mass point were classified as belonging to the 20% group; the 40% of cells closest to the center-mass point as belonging to the 40% group, etc.). Next, the original R-C and ML coordinates for each cell were used to plot all individual cells on a two-dimensional space representing the flattened cerebral cortex, using a custom-made Matlab-based program. Finally, the absolute area occupied by each group of cells within this two-dimensional space was measured.

For the analysis of the tangential dispersion of $GFP^+/BrdU^+$ and $BrdU^+$ transplanted neurons in P0 animals, we plotted with Neurolucida software all cells found in somatosensory and visual cortex near these two levels: 3.2 and 5.2 mm, from the rostral end of the brain.

For the analysis of cortical expansion on embryonic brains (E12.5 and E15.5), we measured the R-C cortical distance on similar sagittal brain sections images from the Allen Brain Institute.

Mathematical model

For the mathematical model, we first measured the cortical length at different stages, namely, E12.5, E15.5, E17.5 and P1.5, obtaining measurements of

Development (2020) 147, dev185033. doi:10.1242/dev.185033

2200, 4150, 4900 and 6100 µm, respectively. We calculated the best-fitting polynomial to the absolute expansion of the hemicortex as: $y=-0.0217*x^2+14.185*x+1113.2$; $R^2=0.997$. We used this formula to evaluate the relative expansion of the hemicortex per hour. This value was considered to calculate the movement of a CIN while taking into consideration the cortical expansion. The values of CIN speed were approximated at 20 and 25 µm/h for E12.5 and E15.5 CIN, respectively, based on the speed during *in vitro* migration over flattened cortices.

Statistics

All statistical analyses were performed using SPSS v.15 software (IBM). The statistical significance of a single comparison on continuous data was performed using Student's two-tailed unpaired *t*-test with Welch's correction when required (non-equal variances) or the Mann–Whitney nonparametric test when data did not fit a normal distribution (assessed by Shapiro–Wilk normality test). In the case of a single comparison on continuous data obtained from the same brains, we used Student's two-tailed paired *t*-test after ensuring that data fitted to a normal distribution (assessed by Shapiro–Wilk normality test). For multiple comparison, we used one-way ANOVA with a Bonferroni *post hoc* test after checking that our data fitted to a normal distribution (assessed by Shapiro–Wilk normality test) and the variance of the difference was equal (determined by Levene's test). For multiple comparison of cell density by cortical areas, we used two-way ANOVA, also known as general linear model univariate, for repeated-measures (rANOVA), with a Bonferroni *post hoc* test to determine the significance of principal effects between pairs of independent factor levels after checking that our data fitted to a normal distribution (assessed by Shapiro–Wilk normality test) and the variance of the difference was equal (determined by W. Mauchly's test of sphericity). To examine differences across the R-C and ML distribution of each animal, data were statistically analyzed using the Kolmogorov–Smirnov test, and differences of percentage area occupied by cells were compared using Student's *t*-test. The statistical significance of discrete data was assessed using the χ^2 test. The *n* refers to the number of mice analyzed, unless otherwise stated in the figure legends.

Acknowledgements

We thank Oscar Marin (King's College London) and John L. Rubenstein (University of California, San Francisco) for providing the *Nkx2.1-Cre* and *Rosa 26-YFP* mice and support. We also thank the entire histology department of the Universidad de Castilla-La Mancha and Samuel Pleasure (University of California, San Francisco) for their support and advice. We are grateful to Carmen Navarro González for her help with primary culture of CINs.

Competing interests

The authors declare no competing or financial interests.

Author contributions

Formal analysis: R.P.; Investigation: P.F., N.M., O.Y., D.V., R.P.; Data curation: P.F., N.M., O.Y., D.V.; Writing - original draft: R.P.; Writing - review & editing: P.F., N.M., O.Y., D.V., R.P.; Supervision: R.P.; Project administration: R.P.

Funding

This work was supported by the Ministerio de Economía y Competitividad (RYC-2014-16410 and SAF2017-89020-R to P.F.) and by FEDER (European Regional Development Fund) funds for instrumentation at the Centro de Investigación Príncipe Felipe. We also thank the Conselleria de Sanitat of the Generalitat Valenciana via the Centro de Investigación Príncipe Felipe for support. N.M. is supported by the Horizon 2020 program; O.Y. is supported by the US National Institutes of Health/National Cancer Institute (K01CA201068); D.V. is supported by the Spectrum Health-Michigan State University Alliance Corporation; R.P. is supported by the Ministerio de Educación, Cultura y Deporte of Castile-La-Mancha and the European Union regional development fund (SBPLY/17/180501/000314). Deposited in PMC for release after 12 months.

Supplementary information

Supplementary information available online at
https://dev.biologists.org/lookup/doi/10.1242/dev.185033.supplemental

Peer review history

The peer review history is available online at https://dev.biologists.org/lookup/doi/10.1242/dev.185033.reviewer-comments.pdf

References

Adams, J. C. (1981). Heavy metal intensification of DAB-based HRP reaction product. *J. Histochem. Cytochem.* **29**, 775. doi:10.1177/29.6.7252134

Anderson, S. A., Eisenstat, D. D., Shi, L. and Rubenstein, J. L. (1997). Interneuron migration from basal forebrain to neocortex: dependence on Dlx genes. *Science* **278**, 474-476. doi:10.1126/science.278.5337.474

Anderson, S. A., Kaznowski, C. E., Horn, C., Rubenstein, J. L. and McConnell, S. K. (2002). Distinct origins of neocortical projection neurons and interneurons in vivo. *Cereb. Cortex* **12**, 702-709. doi:10.1093/cercor/12.7.702

Bartolini, G., Ciceri, G. and Marín, O. (2013). Integration of GABAergic interneurons into cortical cell assemblies: lessons from embryos and adults. *Neuron* **79**, 849-864. doi:10.1016/j.neuron.2013.08.014

Batista-Brito, R., Rossignol, E., Hjerling-Leffler, J., Denaxa, M., Wegner, M., Lefebvre, V., Pachnis, V. and Fishell, G. (2009). The cell-intrinsic requirement of Sox6 for cortical interneuron development. *Neuron* **63**, 466-481. doi:10.1016/j.neuron.2009.08.005

Bayer, S. A. and Altman, J. (1991). *Neocortical Development*. New York: Raven Press.

Britto, J. M., Obata, K., Yanagawa, Y. and Tan, S.-S. (2006). Migratory response of interneurons to different regions of the developing neocortex. *Cereb. Cortex* **16** Suppl. 1, i57-i63. doi:10.1093/cercor/bhj173

Celio, M. R. (1990). Calbindin D-28k and parvalbumin in the rat nervous system. *Neuroscience* **35**, 375-475. doi:10.1016/0306-4522(90)90091-H

Ciceri, G., Dehorter, N., Sols, I., Huang, Z. J., Maravall, M. and Marín, O. (2013). Lineage-specific laminar organization of cortical GABAergic interneurons. *Nat. Neurosci.* **16**, 1199-1210. doi:10.1038/nn.3485

del Rio, J. A., de Lecea, L., Ferrer, I. and Soriano, E. (1994). The development of parvalbumin-immunoreactivity in the neocortex of the mouse. *Brain Res. Dev. Brain Res.* **81**, 247-259. doi:10.1016/0165-3806(94)90311-5

Denaxa, M., Kalaitzidou, M., Garefalaki, A., Achimastou, A., Lasrado, R., Maes, T. and Pachnis, V. (2012). Maturation-promoting activity of SATB1 in MGE-derived cortical interneurons. *Cell Rep.* **2**, 1351-1362. doi:10.1016/j.celrep.2012.10.003

Fairén, A., Cobas, A. and Fonseca, M. (1986). Times of generation of glutamic acid decarboxylase immunoreactive neurons in mouse somatosensory cortex. *J. Comp. Neurol.* **251**, 67-83. doi:10.1002/cne.902510105

Fishell, G. and Rudy, B. (2011). Mechanisms of inhibition within the telencephalon: "where the wild things are". *Annu. Rev. Neurosci.* **34**, 535-567. doi:10.1146/annurev-neuro-061010-113717

Flames, N., Long, J. E., Garratt, A. N., Fischer, T. M., Gassmann, M., Birchmeier, C., Lai, C., Rubenstein, J. L. and Marín, O. (2004). Short- and long-range attraction of cortical GABAergic interneurons by neuregulin-1. *Neuron* **44**, 251-261. doi:10.1016/j.neuron.2004.09.028

Flames, N., Pla, R., Gelman, D. M., Rubenstein, J. L. R., Puelles, L. and Marín, O. (2007). Delineation of multiple subpallial progenitor domains by the combinatorial expression of transcriptional codes. *J. Neurosci.* **27**, 9682-9695. doi:10.1523/JNEUROSCI.2750-07.2007

Franco, S. J., Martinez-Garay, I., Gil-Sanz, C., Harkins-Perry, S. R. and Müller, U. (2011). Reelin regulates cadherin function via Dab1/Rap1 to control neuronal migration and lamination in the neocortex. *Neuron* **69**, 482-497. doi:10.1016/j.neuron.2011.01.003

Gelman, D. M. and Marín, O. (2010). Generation of interneuron diversity in the mouse cerebral cortex. *Eur. J. Neurosci.* **31**, 2136-2141. doi:10.1111/j.1460-9568.2010.07267.x

Gelman, D., Griveau, A., Dehorter, N., Teissier, A., Varela, C., Pla, R., Pierani, A. and Marín, O. (2011). A wide diversity of cortical GABAergic interneurons derives from the embryonic preoptic area. *J. Neurosci.* **31**, 16570-16580. doi:10.1523/JNEUROSCI.4068-11.2011

Gil-Sanz, C., Franco, S. J., Martinez-Garay, I., Espinosa, A., Harkins-Perry, S. and Müller, U. (2013). Cajal-Retzius cells instruct neuronal migration by coincidence signaling between secreted and contact-dependent guidance cues. *Neuron* **79**, 461-477. doi:10.1016/j.neuron.2013.06.040

Hadjantonakis, A.-K., Gertsenstein, M., Ikawa, M., Okabe, M. and Nagy, A. (1998). Generating green fluorescent mice by germline transmission of green fluorescent ES cells. *Mech. Dev.* **76**, 79-90. doi:10.1016/S0925-4773(98)00093-8

Hevner, R. F., Daza, R. A. M., Englund, C., Kohtz, J. and Fink, A. (2004). Postnatal shifts of interneuron position in the neocortex of normal and reeler mice: evidence for inward radial migration. *Neuroscience* **124**, 605-618. doi:10.1016/j.neuroscience.2003.11.033

Hof, P. R., Glezer, I. I., Condé, F., Flagg, R. A., Rubin, M. B., Nimchinsky, E. A. and Vogt Weisenhorn, D. M. (1999). Cellular distribution of the calcium-binding proteins parvalbumin, calbindin, and calretinin in the neocortex of mammals: phylogenetic and developmental patterns. *J. Chem. Neuroanat.* **16**, 77-116. doi:10.1016/S0891-0618(98)00065-9

Hu, J. S., Vogt, D., Sandberg, M. and Rubenstein, J. L. (2017). Cortical interneuron development: a tale of time and space. *Development* **144**, 3867-3878. doi:10.1242/dev.132852

Kawaguchi, Y. and Kubota, Y. (1997). GABAergic cell subtypes and their synaptic connections in rat frontal cortex. *Cereb. Cortex* **7**, 476-486. doi:10.1093/cercor/7.6.476

Kessaris, N., Magno, L., Rubin, A. N. and Oliveira, M. G. (2014). Genetic programs controlling cortical interneuron fate. *Curr. Opin. Neurobiol.* **26**, 79-87. doi:10.1016/j.conb.2013.12.012

Kriegstein, A. R. and Noctor, S. C. (2004). Patterns of neuronal migration in the embryonic cortex. *Trends Neurosci.* **27**, 392-399. doi:10.1016/j.tins.2004.05.001

Kubota, Y., Shigematsu, N., Karube, F., Sekigawa, A., Kato, S., Yamaguchi, N., Hirai, Y., Morishima, M. and Kawaguchi, Y. (2011). Selective coexpression of multiple chemical markers defines discrete populations of neocortical GABAergic neurons. *Cereb. Cortex* **21**, 1803-1817. doi:10.1093/cercor/bhq252

Lavdas, A. A., Grigoriou, M., Pachnis, V. and Parnavelas, J. G. (1999). The medial ganglionic eminence gives rise to a population of early neurons in the developing cerebral cortex. *J. Neurosci.* **19**, 7881-7888. doi:10.1523/JNEUROSCI.19-18-07881.1999

Lim, L., Pakan, J. M. P., Selten, M. M., Marques-Smith, A., Llorca, A., Bae, S. E., Rochefort, N. L. and Marín, O. (2018). Optimization of interneuron function by direct coupling of cell migration and axonal targeting. *Nat. Neurosci.* **21**, 920-931. doi:10.1038/s41593-018-0162-9

Lopez-Bendito, G., Sanchez-Alcaniz, J. A., Pla, R., Borrell, V., Pico, E., Valdeolmillos, M. and Marín, O. (2008). Chemokine signaling controls intracortical migration and final distribution of GABAergic interneurons. *J. Neurosci.* **28**, 1613-1624. doi:10.1523/JNEUROSCI.4651-07.2008

Lourenço, M. R., Garcez, P. P., Lent, R. and Uziel, D. (2012). Temporal and spatial regulation of interneuron distribution in the developing cerebral cortex–an in vitro study. *Neuroscience* **201**, 357-365. doi:10.1016/j.neuroscience.2011.10.041

Mardinly, A. R., Spiegel, I., Patrizi, A., Centofante, E., Bazinet, J. E., Tzeng, C. P., Mandel-Brehm, C., Harmin, D. A., Adesnik, H., Fagiolini, M. et al. (2016). Sensory experience regulates cortical inhibition by inducing IGF1 in VIP neurons. *Nature* **531**, 371-375. doi:10.1038/nature17187

Marín, O. (2012). Interneuron dysfunction in psychiatric disorders. *Nat. Rev. Neurosci.* **13**, 107-120. doi:10.1038/nrn3155

Marín, O. (2013). Cellular and molecular mechanisms controlling the migration of neocortical interneurons. *Eur. J. Neurosci.* **38**, 2019-2029. doi:10.1111/ejn.12225

Marín, O. and Rubenstein, J. L. (2001). A long, remarkable journey: tangential migration in the telencephalon. *Nat. Rev. Neurosci.* **2**, 780-790. doi:10.1038/35097509

Marín, O., Valiente, M., Ge, X. and Tsai, L.-H. (2010). Guiding neuronal cell migrations. *Cold Spring Harb. Perspect Biol.* **2**, a001834. doi:10.1101/cshperspect.a001834

Markram, H., Toledo-Rodriguez, M., Wang, Y., Gupta, A., Silberberg, G. and Wu, C. (2004). Interneurons of the neocortical inhibitory system. *Nat. Rev. Neurosci.* **5**, 793-807. doi:10.1038/nrn1519

Martini, F. J., Valiente, M., Lopez Bendito, G., Szabo, G., Moya, F., Valdeolmillos, M. and Marin, O. (2009). Biased selection of leading process branches mediates chemotaxis during tangential neuronal migration. *Development* **136**, 41-50. doi:10.1242/dev.025502

Miyoshi, G., Butt, S. J. B., Takebayashi, H. and Fishell, G. (2007). Physiologically distinct temporal cohorts of cortical interneurons arise from telencephalic Olig2-expressing precursors. *J. Neurosci.* **27**, 7786-7798. doi:10.1523/JNEUROSCI.1807-07.2007

Miyoshi, G. and Fishell, G. (2011). GABAergic interneuron lineages selectively sort into specific cortical layers during early postnatal development. *Cereb. Cortex* **21**, 845-852. doi:10.1093/cercor/bhq155

Miyoshi, G., Hjerling-Leffler, J., Karayannis, T., Sousa, V. H., Butt, S. J., Battiste, J., Johnson, J. E., Machold, R. P. and Fishell, G. (2010). Genetic fate mapping reveals that the caudal ganglionic eminence produces a large and diverse population of superficial cortical interneurons. *J. Neurosci.* **30**, 1582-1594. doi:10.1523/JNEUROSCI.4515-09.2010

Nadarajah, B. and Parnavelas, J. G. (2002). Modes of neuronal migration in the developing cerebral cortex. *Nat. Rev. Neurosci.* **3**, 423-432. doi:10.1038/nrn845

Nery, S., Fishell, G. and Corbin, J. G. (2002). The caudal ganglionic eminence is a source of distinct cortical and subcortical cell populations. *Nat. Neurosci.* **5**, 1279-1287. doi:10.1038/nn971

Nóbrega-Pereira, S. and Marin, O. (2009). Transcriptional control of neuronal migration in the developing mouse brain. *Cereb. Cortex* **19** Suppl. 1, i107-i113. doi:10.1093/cercor/bhp044

Nóbrega-Pereira, S., Kessaris, N., Du, T., Kimura, S., Anderson, S. A. and Marín, O. (2008). Postmitotic Nkx2-1 controls the migration of telencephalic interneurons by direct repression of guidance receptors. *Neuron* **59**, 733-745. doi:10.1016/j.neuron.2008.07.024

Ouellet, L. and de Villers-Sidani, E. (2014). Trajectory of the main GABAergic interneuron populations from early development to old age in the rat primary auditory cortex. *Front. Neuroanat.* **8**, 40. doi:10.3389/fnana.2014.00040

Pai, E. L.-L., Vogt, D., Clemente-Perez, A., McKinsey, G. L., Cho, F. S., Hu, J. S., Wimer, M., Paul, A., Fazel Darbandi, S., Pla, R. et al. (2019). *Mafb* and *c-Maf* have prenatal compensatory and postnatal antagonistic roles in cortical interneuron fate and function. *Cell Reports* 26, 1157-1173.e5. doi:10.1016/j.celrep.2019.01.031

Pla, R., Borrell, V., Flames, N. and Marin, O. (2006). Layer acquisition by cortical GABAergic interneurons is independent of Reelin signaling. *J. Neurosci.* **26**, 6924-6934. doi:10.1523/JNEUROSCI.0245-06.2006

Polleux, F., Whitford, K. L., Dijkhuizen, P. A., Vitalis, T. and Ghosh, A. (2002). Control of cortical interneuron migration by neurotrophins and PI3-kinase signaling. *Development* **129**, 3147-3160.

Pozas, E. and Ibáñez, C. F. (2005). GDNF and GFRα1 promote differentiation and tangential migration of cortical GABAergic neurons. *Neuron* **45**, 701-713. doi:10.1016/j.neuron.2005.01.043

Rubin, A. N., Alfonsi, F., Humphreys, M. P., Choi, C. K., Rocha, S. F. and Kessaris, N. (2010). The germinal zones of the basal ganglia but not the septum generate GABAergic interneurons for the cortex. *J. Neurosci.* **30**, 12050-12062. doi:10.1523/JNEUROSCI.6178-09.2010

Sanchez-Alcaniz, J. A., Haege, S., Mueller, W., Pla, R., Mackay, F., Schulz, S., Lopez-Bendito, G., Stumm, R. and Marin, O. (2011). Cxcr7 controls neuronal migration by regulating chemokine responsiveness. *Neuron* **69**, 77-90. doi:10.1016/j.neuron.2010.12.006

Southwell, D. G., Paredes, M. F., Galvao, R. P., Jones, D. L., Froemke, R. C., Sebe, J. Y., Alfaro-Cervello, C., Tang, Y., Garcia-Verdugo, J. M., Rubenstein, J. L. et al. (2012). Intrinsically determined cell death of developing cortical interneurons. *Nature* **491**, 109-113. doi:10.1038/nature11523

Srinivas, S., Watanabe, T., Lin, C.-S., William, C. M., Tanabe, Y., Jessell, T. M. and Costantini, F. (2001). Cre reporter strains produced by targeted insertion of EYFP and ECFP into the ROSA26 locus. *BMC Dev. Biol.* **1**, 4. doi:10.1186/1471-213X-1-4

Taniguchi, H., He, M., Wu, P., Kim, S., Paik, R., Sugino, K., Kvitsani, D., Fu, Y., Lu, J., Lin, Y. et al. (2011). A resource of cre driver lines for genetic targeting of GABAergic neurons in cerebral cortex. *Neuron* **71**, 995-1013. doi:10.1016/j.neuron.2011.07.026

Torigoe, M., Yamauchi, K., Kimura, T., Uemura, Y. and Murakami, F. (2016). Evidence that the laminar fate of LGE/CGE-derived neocortical interneurons is dependent on their progenitor domains. *J. Neurosci.* **36**, 2044-2056. doi:10.1523/JNEUROSCI.3550-15.2016

Touzot, A., Ruiz-Reig, N., Vitalis, T. and Studer, M. (2016). Molecular control of two novel migratory paths for CGE-derived interneurons in the developing mouse brain. *Development* **143**, 1753-1765. doi:10.1242/dev.131102

Tremblay, R., Lee, S. and Rudy, B. (2016). GABAergic interneurons in the neocortex: from cellular properties to circuits. *Neuron* **91**, 260-292. doi:10.1016/j.neuron.2016.06.033

Valcanis, H. and Tan, S.-S. (2003). Layer specification of transplanted interneurons in developing mouse neocortex. *J. Neurosci.* **23**, 5113-5122. doi:10.1523/JNEUROSCI.23-12-05113.2003

Villar-Cerviño, V., Molano-Mazón, M., Catchpole, T., Valdeolmillos, M., Henkemeyer, M., Martínez, L. M., Borrell, V. and Marin, O. (2013). Contact repulsion controls the dispersion and final distribution of Cajal-Retzius cells. *Neuron* **77**, 457-471. doi:10.1016/j.neuron.2012.11.023

Vogt, D., Hunt, R. F., Mandal, S., Sandberg, M., Silberberg, S. N., Nagasawa, T., Yang, Z., Baraban, S. C. and Rubenstein, J. L. R. (2014). Lhx6 directly regulates Arx and CXCR7 to determine cortical interneuron fate and laminar position. *Neuron* **82**, 350-364. doi:10.1016/j.neuron.2014.02.030

Wonders, C. P. and Anderson, S. A. (2006). The origin and specification of cortical interneurons. *Nat. Rev. Neurosci.* **7**, 687-696. doi:10.1038/nrn1954

Wonders, C. P., Taylor, L., Welagen, J., Mbata, I. C., Xiang, J. Z. and Anderson, S. A. (2008). A spatial bias for the origins of interneuron subgroups within the medial ganglionic eminence. *Dev. Biol.* **314**, 127-136. doi:10.1016/j.ydbio.2007.11.018

Xu, Q., Tam, M. and Anderson, S. A. (2008). Fate mapping Nkx2.1-lineage cells in the mouse telencephalon. *J. Comp. Neurol.* **506**, 16-29. doi:10.1002/cne.21529

Xu, X., Roby, K. D. and Callaway, E. M. (2010). Immunochemical characterization of inhibitory mouse cortical neurons: Three chemically distinct classes of inhibitory cells. *J. Comp. Neurol.* **518**, 389-404. doi:10.1002/cne.22229

Yozu, M., Tabata, H. and Nakajima, K. (2005). The caudal migratory stream: a novel migratory stream of interneurons derived from the caudal ganglionic eminence in the developing mouse forebrain. *J. Neurosci.* **25**, 7268-7277. doi:10.1523/JNEUROSCI.2072-05.2005

Zimmer, G., Garcez, P., Rudolph, J., Niehage, R., Weth, F., Lent, R. and Bolz, J. (2008). Ephrin-A5 acts as a repulsive cue for migrating cortical interneurons. *Eur. J. Neurosci.* **28**, 62-73. doi:10.1111/j.1460-9568.2008.06320.x

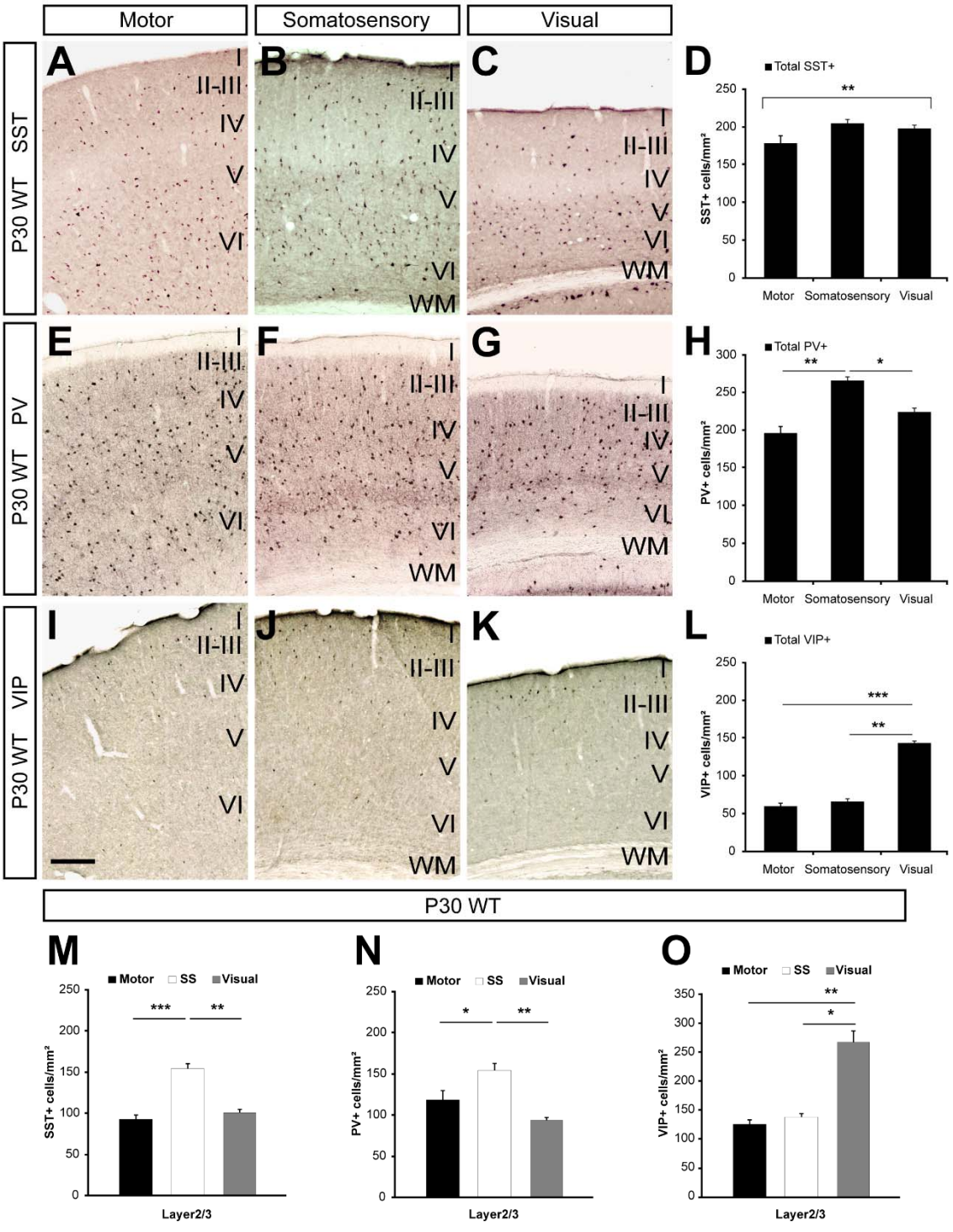

Fazzari et al. Suplementary Fig1

Fig. S1. SST+ and PV+ cells density changes between cortical areas in upper layers.

A-C, E-G, I-K, Microscope images from coronal sections of (A, E, I) motor, (B, F, J) somatosensory and (C, G, K) visual cortex of P30 wild type mice displaying the distribution of (A-C) SST, (E-G) PV and (I-K) VIP expressing cells. D, H, L Quantification of cells density of (D) SST+ (motor: 178.49 ±9.76 cells/mm^2; somatosensory: 204.85 ±4.8 cells/mm^2; visual: 197.75 ±5.7 cells/mm^2, p=0.006, n=4), (H) PV+ (motor: 194.91 ±10.18 cells/mm^2; somatosensory: 265.26 ±5 cells/mm^2; visual: 223.53 ±5.1 cells/mm^2, p=0.001, n=5) and (L) VIP+ (motor: 58.58 ±4.46 cells/mm^2; somatosensory: 65.9 ±3.73 cells/mm^2; visual: 142.9 ±2.9 cells/mm^2, p=6.8x10^{-6}, n=4) cells in motor, SS and visual cortex. M-O Quantification of cells density in layer 2/3 in motor (black bar), SS (white bar) and visual (gray bar) cortex of (M) SST+ (motor: 91.79 ±4.82 cells/mm^2; somatosensory: 153.87 ±5.87 cells/mm^2; visual: 99.98 ±4.2 cells/mm^2, p=3.5x10^{-5}, n=4), (N) PV+ (motor: 118.84 ±10.99 cells/mm^2; somatosensory: 154.40 ±8.9 cells/mm^2; visual: 93.81 ±3.7 cells/mm^2, p=0.001, n=5) and (O) VIP+ (motor: 126.16 ±7.3 cells/mm^2; somatosensory: 138.35 ±5.3 cells/mm^2; visual: 267.5 ±19.7 cells/mm^2, p=0.0003, n=4). *p<0.05, **p<0.01 and ***p<0.01 (rANOVA, test). Histograms show average ±SEM. SST, somatostatin; PV, parvalbumin; VIP, vasointestinal peptide. Scale bar, 200 μm.

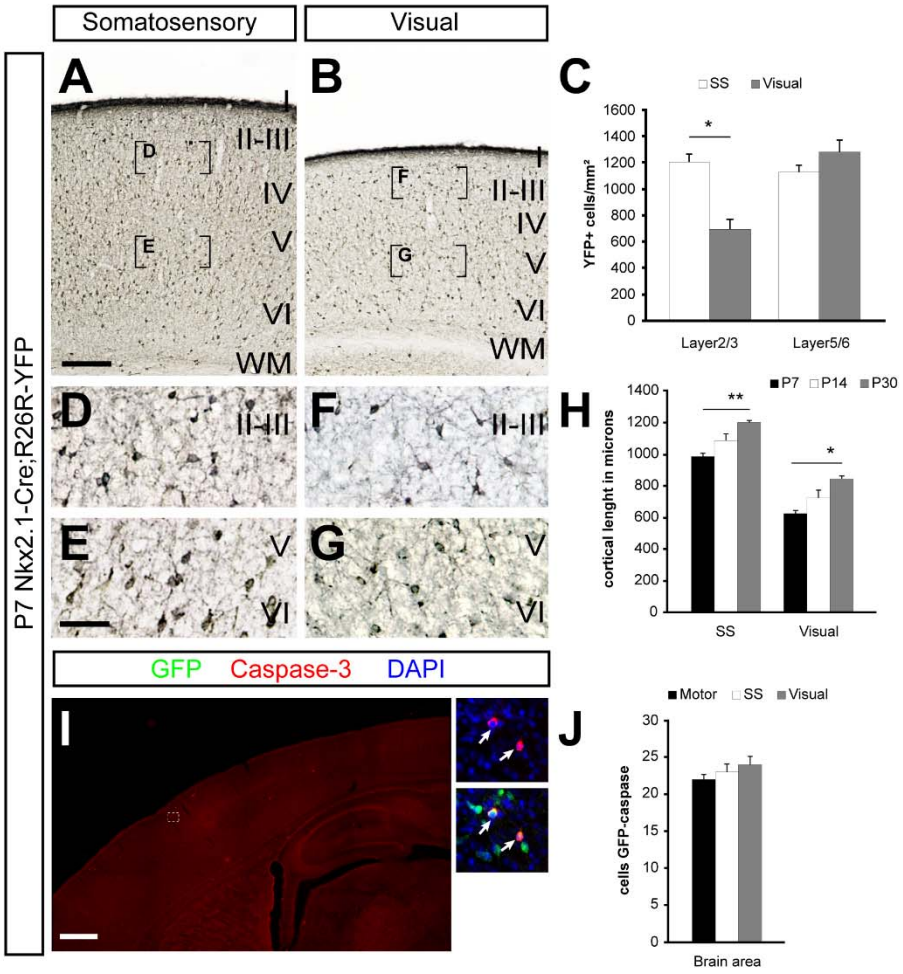

Fazzari et al., Suplementary Fig2

Fig. S2. Differences in the distribution of MGE-derived CINs along the cortex of *Nkx2-1- Cre;R26R-YFP* mice are already present at P7 and are independent of cell death.

A,B, Coronal section through the somatosensory (A) and visual (B) cortex of P7 *Nkx2-1-Cre;R26R-YFP* mice showing the distribution of YFP-expressing cells after YFP staining. D-G, High magnification images of the bracket areas shown in A and B. Note that whereas YFP-expressing cells are equally distribute in deeper layers of somatosensory (E) and visual (G) cortex, YFP-expressing cells are more abundant in upper layers of somatosensory (D) cortex in compare of visual (F) cortex. C, Quantification of the distribution of YFP-expressing cells in somatosensory (white bars) and visual (gray bars) cortex, (Layer 2/3, somatosensory: 1191.83 ±66.66 cells/mm^2; visual: 688.34 ±81.32 cells/mm^2, p=0.035; Layer 5/6, somatosensory: 1121.74 ±53.84 cells/mm^2; visual: 1271.34 ±90.60 cells/mm^2, p=0.34, n=3). H, Quantification of cortical length at P7, (black bars), P14 (white bars) and P30 (gray bars) in somatosensory (P7: 980 ±21.9 microns; P14: 1081 ±42.3 microns; P30: 1195.7 ±11.6 microns, p=0.005, n=3) and visual cortex (P7: 628.47 ±16.8 microns; P14: 720.15 ±49.9 microns; P30: 835.97 ±22.2 microns, p=0.012, n=3). I, Sagittal section through the cortex of P7 *Nkx2-1- Cre;R26R-YFP* mice showing the distribution of dying cells after Caspase (red) and YFP (green) staining (see insets). J, Quantification of the distribution of *Nkx2-1- Cre* dead cells in the motor, somatosensory and visual cortex, (motor: 22 ±0.5 cells; somatosensory: 23 ±0.7 cells; visual: 24 ±1.1 cells, p=0.96, n=5). *p<0.05 and **p<0.01 (ANOVA, paired Student's *t*-test and χ^2 test) Histograms show average ±SEM. SS, somatosensory. Scale bar (in A) A-B 200 μm; (in E) D-G, 50 μm.

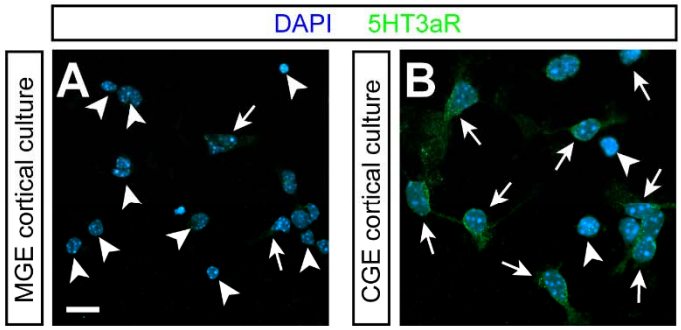

Fazzari et al., Supplementary Fig3

Fig. S3. MGE cortical culture contains some CGE-derived CINs.

A-B, Confocal images of dissociated cultures obtained from E15.5 CGE (A) and MGE (B) of WT embryos stained for a nuclear staining [4_,6_-diamidino-2-phenylindole dihydrochloride (DAPI)] and immunohistochemistry for 5HT3 (MGE:9 out of 76; CGE:62 out of 70) Arrows point to 5HT3+ cells and arrowheads point 5HT3 negative cells. Scale bar (in A) A-B, 10 μm.

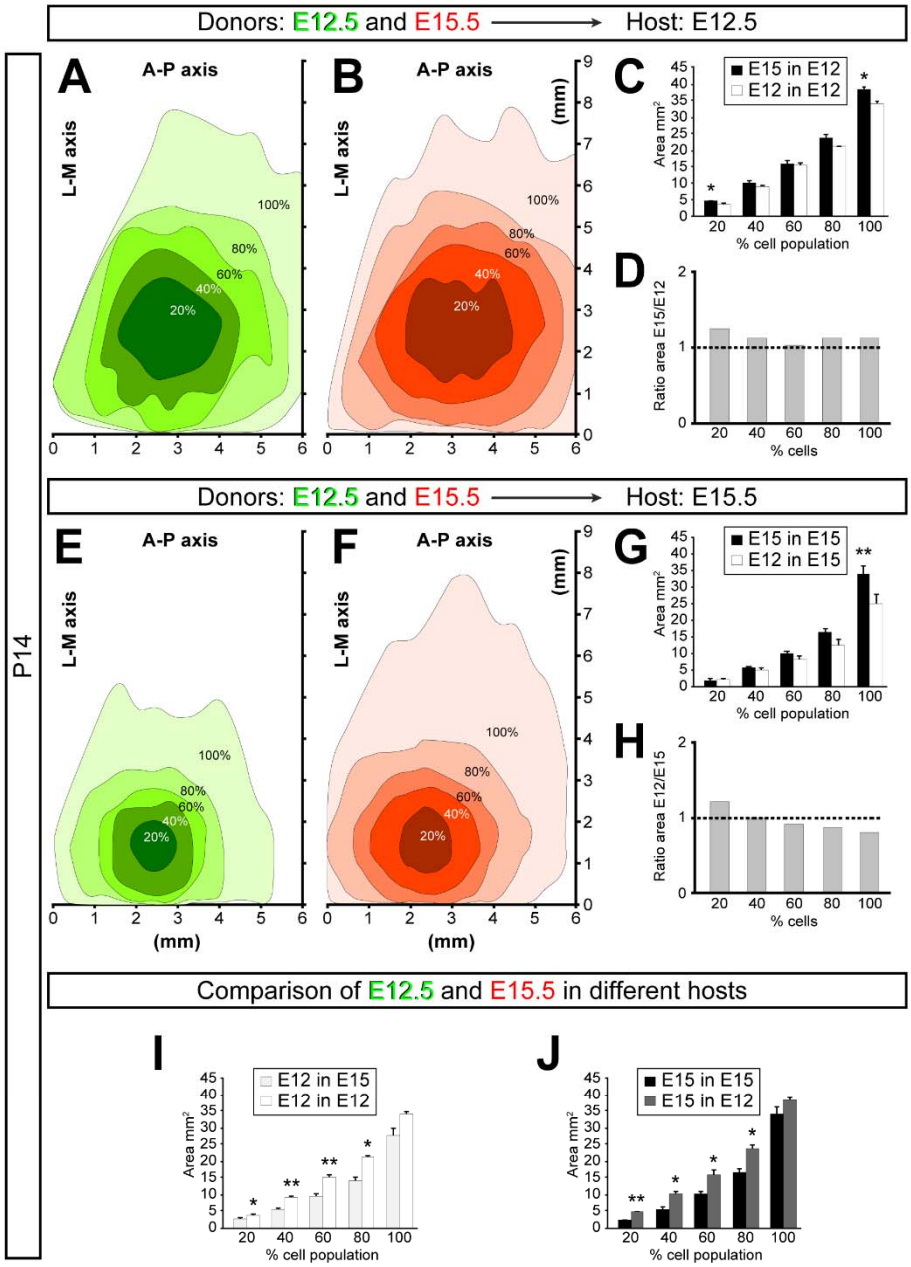

Fazzari et al., Suplementary Fig4

Fig. S4. Timing is essential for a correct cortical distribution.

A, B, E, F, Density maps showing the distribution in the P14 cortex of E12.5 (A, E) and E15.5 (B, F) interneurons injected in E12.5 (A-B) or E15.5 (E-F) host embryos. Each colored-coded area (green or red) contains an increasingly higher proportion of the entire population of transplanted neurons, from 20% (darkest colored area) to 100% (lightest colored area). L-M, Lateral–medial; A-P, anteroposterior. C, Quantification in the P14 cortex of the cortical area occupied by transplanted E15 (filled bars) and E12 (open bars) interneurons in E12.5 host embryos (20%, E15: 4.84 ±0.1 mm^2; E12: 3.87 ±0.3 mm^2, n=4; p=0.03; 40%, E15: 10.27 ±0.9 mm^2; E12: 9.1 ±0.4 mm^2, n=3; p=0.3; 60%, E15: 15.87 ±1.8 mm^2; E12: 15.46 ±0.8 mm^2, n=3; p=0.8; 80%, E15: 23.87 ±1.4 mm^2; E12: 21.27 ±0.4 mm^2, n=3; p=0.2; 100%, E15: 38.33 ±1 mm^2; E12: 34.15 ±0.7 mm^2, n=3; p=0.02). D, Quantification of the relative cortical area occupied by transplanted E15 and E12 interneurons in the P14 cortex. G, Quantification in the P14 cortex of the cortical area occupied by transplanted E15 (filled bars) and E12 (open bars) interneurons in E15.5 host embryos (20%, E15: 2.19 ±0.4 mm^2; E12: 2.10 ±0.6 mm^2, n=3; p=0.6; 40%, E15: 5.7 ±0.5 mm^2; E12: 4.96 ±0.8 mm^2, n=3; p=0.2; 60%, E15: 10.16 ±0.8 mm^2; E12: 8.16 ±1.3 mm^2, n=3; p=0.06; 80%, E15: 16.56 ±1 mm^2; E12: 12.81 ±1.6 mm^2, n=3; p=0.12; 100%, E15: 34.15 ±2.3 mm^2; E12: 24.89 ±2.9 mm^2, n=3; p=0.007). H, Quantification of the relative cortical area occupied by transplanted E12 and E15 interneurons in the P14 cortex. I, Quantification of the relative cortical area occupied by transplanted E12 and E15 interneurons in E12 and E15 respectively hosts. J, comparison of the cortical area occupied by E12 interneurons transplanted in E15 (gray bars) or E12 (white bars) from data shown in D and H. K, comparison of the cortical area occupied by E15 interneurons transplanted in E15 (black bars) or E12 (gray bars) from data shown in D and H. *p<0.05, **p<0.01, (Kolmogorov-Smirnov and paired Student's t-test). Histograms show average ±SEM.

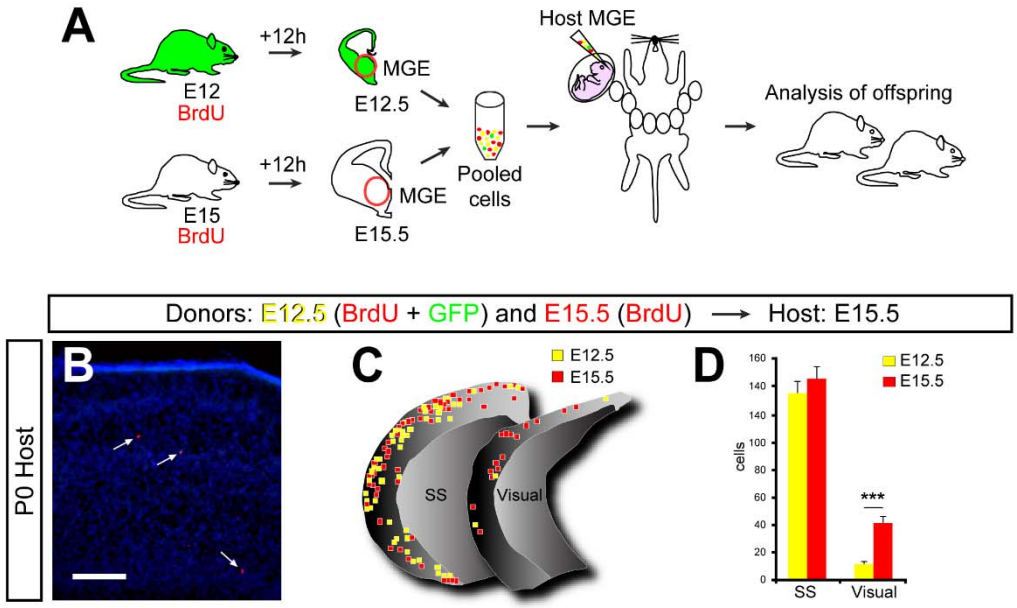

Fazzari et al. Suplementary Fig5

Fig. S5. Heterochronic transplants show differences in cell migration at early postnatal stages.

A, Schema of the experimental design followed in B-D. GFP+ donor pregnant received a single injection of BrdU at E12 and wild type donor pregnant mice received a single injection of Brdu at E15. Twelve hours after BrdU injection, the MGE was dissected from embryos and dissociated. Pooled donor MGE cells were then injected into the MGE of E15.5 host embryos. Host embryos were analyzed at P0. B, Coronal section through the visual cortex of a P0 wild type mouse showing the distribution of BrdU+ and BrdU/GFP+ cells after immunohistochemistry. Arrows point to BrdU+/GFP+ cells. C, Neurolucida drawings comparing the distribution of E12.5 born cells (yellow squares) and E15.5 born cells (red squares) in the somatosensory and visual P0 cortex. Note that whereas E12.5 cells are abundant in somatosensory cortex, very few of them are found in visual cortex. D, Quantification of E12.5 (yellow bars) and E15.5 (red bars) born cells at somatosensory and visual cortex. (E12.5, somatosensory: 406 cells; visual: 36; E15.5, somatosensory: 437 cells; visual: 125, p=1.51x10^{-9}, n=3). ***p<0.001 (χ^2 test). Histograms show average of total cells number ±SEM. SS, somatosensory. Scale bar, 100 μm.

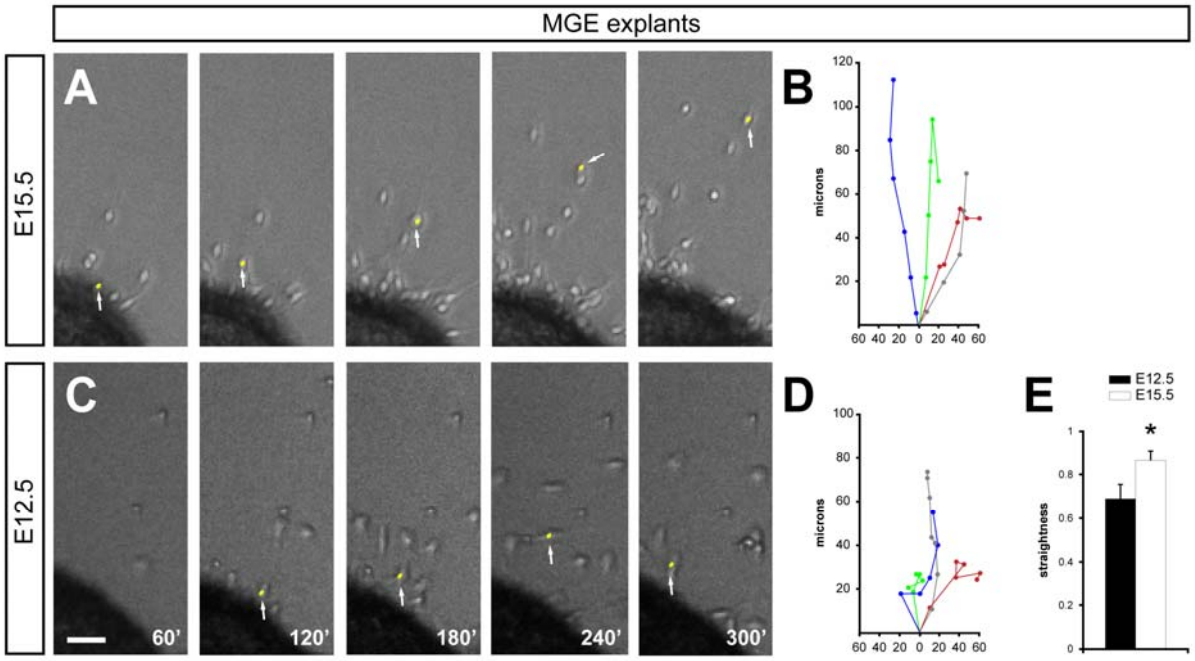

Fazzari et al., Supplementary Fig 6

Fig. S6. Early and late born MGE-derived cells display differences in their migratory trajectories.

A, C, Time-lapse sequence of (A) late and (C) early born MGE-derived cells migrating out of the explant in culture. Time is indicated in minutes. Arrowheads indicate a cell in different time frames and yellow dots indicate the position of the nucleus in each nucleokinesis. B, D, Drawings of the trajectories followed by different representative cells from (B) late and (D) early born MGE explants. E, Quantification of the straightness expressed as the ratio between the distance from the initial point of migration and the total distance covered, of E12.5 born cells (black bar) and E15.5 born cells (white bar) in collagen explant assays, (E12.5: 0.69 ±0.07, *n*=16; E15.5: 0.87 ±0.04, *n*=18; *p*=0.39). 0 maximum tortuosity; 1 maximum straightness. *$p<0.05$, (Mann-Whitney test). Histograms show average of straightness ±SEM. Scale bar, 20 μm.

Movie 1: E12-born MGE-derived cells.
Time-lapse movie of MGE explant in methylcellulose of E12.5-born cells, cultured and record overnight.

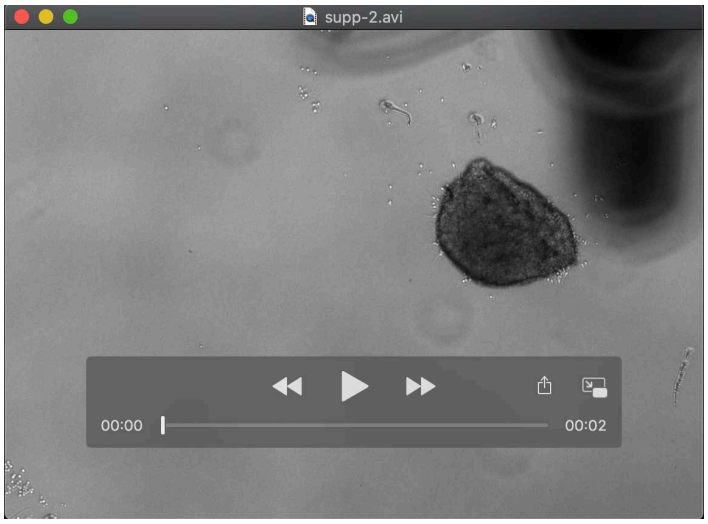

Movie 2: E15-born MGE-derived cells.
Time-lapse movie of MGE explant in methylcellulose of E15.5-born cells, cultured and record overnight.